The Pennsylvania State University

The Graduate School

Department of Aerospace Engineering

DETERMINATION OF OPTIMAL EARTH-MARS TRAJECTORIES TO TARGET THE MOONS OF MARS

A Thesis in

Aerospace Engineering

by

Davide Conte

Submitted in Partial Fulfillment
of the Requirements
for the Degree of

Master of Science

May 2014

The thesis of Davide Conte was reviewed and approved* by the following:

David B. Spencer
Professor of Aerospace Engineering
Thesis Advisor

Robert G. Melton
Professor of Aerospace Engineering
Director of Undergraduate Studies

George A. Lesieutre
Professor of Aerospace Engineering
Head of the Department of Aerospace Engineering

*Signatures are on file in the Graduate School

ABSTRACT

The focus of this thesis is to analyze interplanetary transfer maneuvers from Earth to Mars in order to target the Martian moons, Phobos and Deimos. Such analysis is done by solving Lambert's Problem and investigating the necessary targeting upon Mars arrival. Additionally, the orbital parameters of the arrival trajectory as well as the relative required ΔVs and times of flights were determined in order to define the optimal departure and arrival windows for a given range of date. The first step in solving Lambert's Problem consists in finding the positions and velocities of the departure (Earth) and arrival (Mars) planets for a given range of dates. Then, by solving Lambert's problem for various combinations of departure and arrival dates, porkchop plots can be created and examined. Some of the key parameters that are plotted on porkchop plots and used to investigate possible transfer orbits are the departure characteristic energy, C3, and the arrival v_∞. These parameters, in combination with given desired initial and final parking orbital conditions about Earth and Mars, were also used to determine the total ΔV for the various Earth-Mars transfers. ΔV results were used to find the necessary amount of propellant needed for the transfer maneuvers as a percentage of total spacecraft mass for a given specific impulse. Moreover, this thesis considers the arrival trajectories of an arbitrary spacecraft with respect to a Mars inertial reference frame. Key parameters are the inclination of the arrival orbit with respect to the Mars equator and ΔV needed to be captured by Mars and be inserted in the Martian moons' orbital planes. Lastly, rendezvous maneuvers with Phobos/Deimos are considered.

The results of the analysis lead to the optimal choice of departure and arrival dates that, given the capabilities of the launch system such as ΔV, makes the mission physically feasible.

TABLE OF CONTENTS

LIST OF FIGURES

LIST OF TABLES

LIST OF SYMBOLS

Symbol	***Units***	***Description***
I_{sp}	s	Specific impulse
g_{SL}	m/s^2	Acceleration due to gravity at sea level on Earth
$\hat{n}$	N/A	Node vector
DEC	rad or deg	Declination
RA	rad or deg	Right ascension
$C3$	km^2/s^2	Characteristic energy
E	rad or deg	Eccentric anomaly
TOF	s or $days$	Time of flight
a	km or AU	Semi-major axis
e	N/A	Eccentricity
$f, g, \dot{f}, \dot{g}$	N/A, s, s^{-1}, N/A	Lagrange coefficients
h	km^2/s	Specific angular momentum
i	rad or deg	Inclination
m	kg	Mass of spacecraft and mass of propellant
p	km	Semilatus rectum
r	km or AU	Radial position
t, T	s or $days$	Time
v	km/s or AU/day	Velocity
Ω	rad or deg	Right ascension of the ascending node
α	rad	Auxiliary angle for Lambert's problem

β	rad	Auxiliary angle for Lambert's problem
δ	rad or deg	Turn angle
ε	km^2/s^2	Specific energy
θ	rad or deg	True anomaly
μ	km^3/s^2	Gravitational parameter
χ	$km^{1/2}$	Universal anomaly
ω	rad or deg	Argument of periapsis
ϵ	rad or deg	Obliquity

ACKNOWLEDGEMENTS

I would like to thank Dr. Spencer for all of the help he gave me in writing both my undergraduate and graduate theses, and especially for teaching Interplanetary Astrodynamics, one of the most exciting classes I have taken at Penn State.

I would also like to acknowledge Dr. Melton and Dr. Lesieutre for the teachings and advices they have given me throughout my college career.

Additionally, I would like to thank Dr. Parsons who has given me the mathematical foundations and the support to succeed in my later years at Penn State.

Since I was a child, my dad would take me outside on our balcony and show me the splendors of the universe through the lenses of our telescope. Soon, the love for space my family had given me combined with the passion for science, mathematics, and engineering made me realize that I wanted to make a difference in the future of space exploration. Everything I have worked on, especially during the past five years, was made possible by my parents, Giovanni and Rossana, and my sister, Lucia. Their love and financial support have given me the opportunity to study thousands of miles away from home in one of the best universities in the world. And while I occasionally doubted my own abilities, they never did. Lucia, mamma e papà, grazie di cuore per tutto ciò che avete fatto per me, per gli aiuti morali ed economici che mi avete dato, per i consigli che ho ricevuto nei momenti difficili e per la gioia che mi date quando ci sentiamo e vediamo su internet e soprattutto per la gioia che mi date quando torno a casa in Italia. Anche se forse vi verrà difficile capire alcune delle loro parti, vi dedico le due tesi che ho fatto quest'anno.

I also would like to thank Sour Roberta, my elementary school teacher, who has supported me with her prayers and thoughts.

A special thanks goes to the many friends I have made in America since I started studying abroad. Dedico entrambe le mie tesi anche ai miei amici italiani. Grazie per il vostro supporto e per la vostra ineguagliabile amicizia.

Finally, I would like to thank all of the engineers, scientists, and technicians who work towards space exploration and towards answering the fundamental questions of our seemingly infinite Universe. Their work is an inspiration for me and gives me hope that seeing humans walk on the surface of Mars and other celestial bodies will soon become a reality.

Chapter 1

Introduction

Humanity has always had the desire to explore. In fact, exploration is indeed found within the innate sense of curiosity and enthusiasm that mankind possesses. From religious meaning, depicted as the angry god of war, to astronomical interest because of its strange and apparent retrograde motion, Mars, also known as the red planet, is still considered a remote destination, yet to be reached by humans. In order to fully understand and answer some of the fundamental questions about the formation of our Solar System and the development of life on our planet, interplanetary space exploration has gradually become a necessity.

Due to budget pressures, space mission cost has become a more important key factor in deciding whether a mission will take place. In fact, the cost of unmanned space missions to Mars ranges from a few hundreds millions to billions of USD. For example, the Mars Science Laboratory (MSL) was $2.5 billion USD.[3] Additionally, traditional chemical propulsion systems having a specific impulse (Isp) of 300-350 seconds require 80-85% of the total spacecraft mass to be propellant, allowing only for relatively small payloads to be delivered to Mars. Therefore, it is clear that it is necessary to make propellant-efficient decisions starting from the orbital trajectory design. Optimal trajectories will not only reduce the cost of missions to Mars, but they will also allow for more massive payloads to be transported in orbit around and possibly land on the red planet.

Another challenge humans will have to face when travelling to Mars is represented by the presence of an atmosphere around the planet. The Martian atmospheric density is only about 1% of that of Earth making the entry, descent and landing (EDL) process for large payloads

particularly difficult. Perhaps a first approach to missions to Mars will be represented by landing on one of the moons of Mars, Phobos or Deimos, and conduct experiments from them. In fact, neither moon possesses an atmosphere, making EDL and ascent to orbit an easier task for both unmanned and manned missions. Additionally, rovers that nowadays survey the surface of the red planet require a rather long amount of time to safely plan their route from point A to point B and to communicate back to Earth. In fact, the Round Trip Light Time (RTLT) between a robotic mission to Mars and Earth ranges from about 10 to 40 minutes. Instead, having humans on one of the moons to control robotic missions on the surface of Mars would drastically lower the time delays between rovers and humans making such missions more science-profitable in a shorter amount of time.

Additionally, Phobos and/or Deimos missions can be made feasible for humans by minimizing the required ΔV budget. In fact, according to the SETI Institute, the presence of humans in Mars missions are fundamental since "humans should conduct high priority science activities that are not performed well by robots." [9] According to Hopkins and Pratt:

> "A human mission to one of the two moons of Mars has been suggested as an easier precursor before a mission to land on Mars itself. Astronauts would explore the moon in person and teleoperate rovers on the surface of Mars with minimal lag time, returning samples to Earth." [5]

This thesis presents a method of determining the interplanetary transfer orbit key parameters, including the required ΔVs to achieve the Earth-Mars trajectories that are being analyzed, and the payload to propellant mass ratio. User defined conditions include departure and arrival dates, Earth and Mars parking orbits altitudes, and specific impulse. From these results, optimal departure and arrival dates in order to target the moons of Mars are determined as well as the necessary ΔV and other key features of the arrival hyperbolic orbit about Mars.

Targeting the moons of Mars

Although various mission scenarios to Phobos and Deimos have been proposed in the past, no actual mission ever successfully flew to either of the moons. The mission Phobos-Grunt, a combined effort of the Russian and Chinese space agencies, had the purpose to fly to Mars, deploy a Chinese orbiter (YH-1) around the planet, and return a regolith sample from Phobos. Unfortunately, the probe failed to leave Earth's orbit after launching in November 2012. According to the National Centre for Space Studies (CNES), the maneuvers required to rendezvous with Phobos upon arrival at Mars would have taken up to nine months and five or six orbit corrections would have to be conducted. One primary factor which dictates such an extended timeframe is communication windows between the probe and mission control. [16] Phobos-Grunt did not plan on arriving with an inclination close to that of the orbital plane of Phobos, but rather gradually adjust the spacecraft's orbit while tracking the position of Phobos. Figure 1 illustrates the mission architecture of Phobos-Grunt.

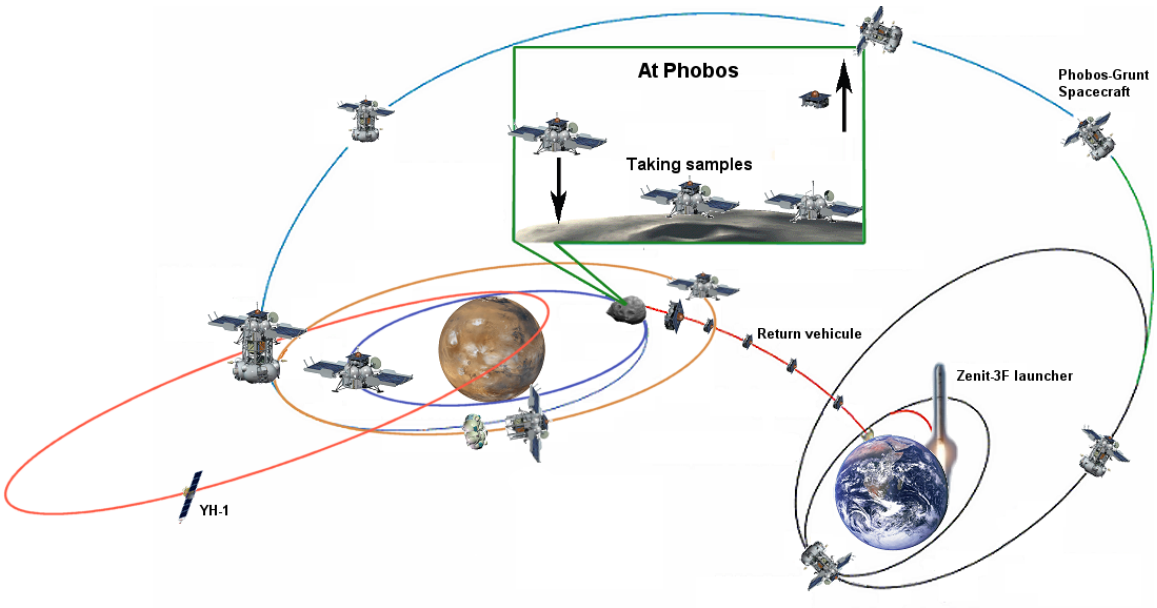

Figure 1 – Phobos-Grunt Mission architecture. Source: CNES. [16]

Besides the mission architecture proposed by Phobos-Grunt, various other scenarios exist for missions to the moons of Mars. For example, Hopkins and Pratt suggest a method based mostly on conducting orbital maneuvers at arrival rather than targeting the plane in which Phobos and Deimos lie. First of all, Hopkins defines a time window during which such a mission should occur based on the minimal predicted solar activity and the optimal launch windows to launch to Mars. Both events roughly happen at the same time in the 2033-2035 range as shown in Figure 2.[5,6]

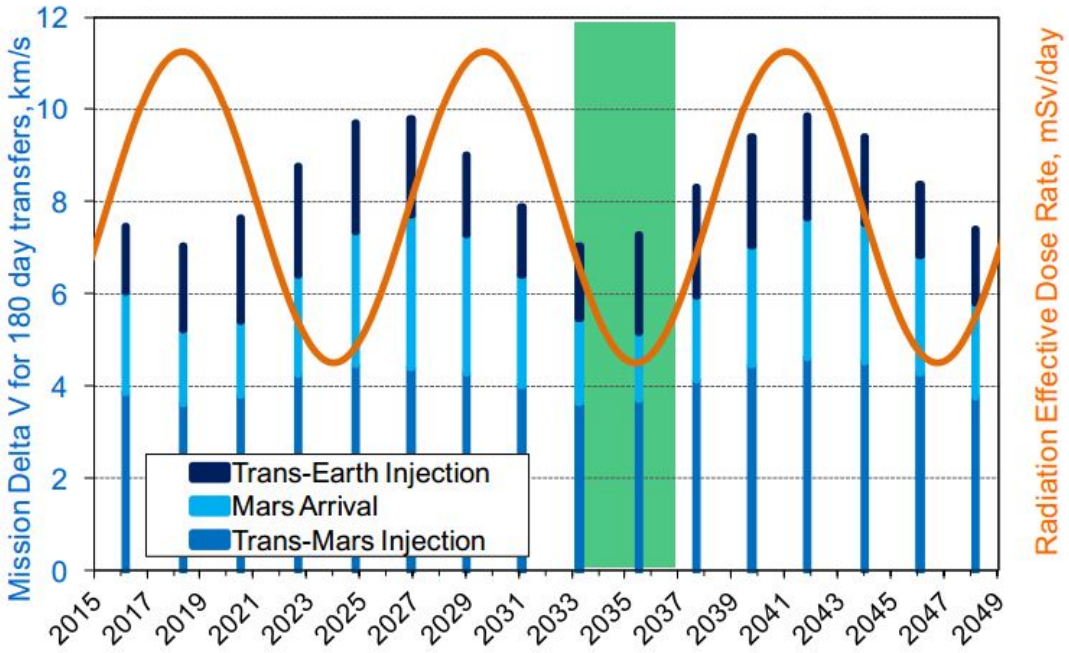

Figure 2 – Optimum phases of 15 year orbital mechanics cycle and 11 year solar cycle (which protects from cosmic rays) probably coincide in 2033-2035. Source: Hopkins. [5,6]

The main idea of the mission design proposed in Hopkins' article is to execute a bi-elliptic burn with plane changes upon arrival at Mars, regardless of what the arrival inclination is with respect to the equatorial plane of Mars. In fact, the first maneuver would correspond to the orbit insertion, then an orbital plane change would be executed at apoapsis (assuming this coincides with the direction of the node vector); lastly, periapsis would be raised so that either

Phobos or Deimos can be correctly intercepted by the spacecraft. Figure 3 shows such mission design.

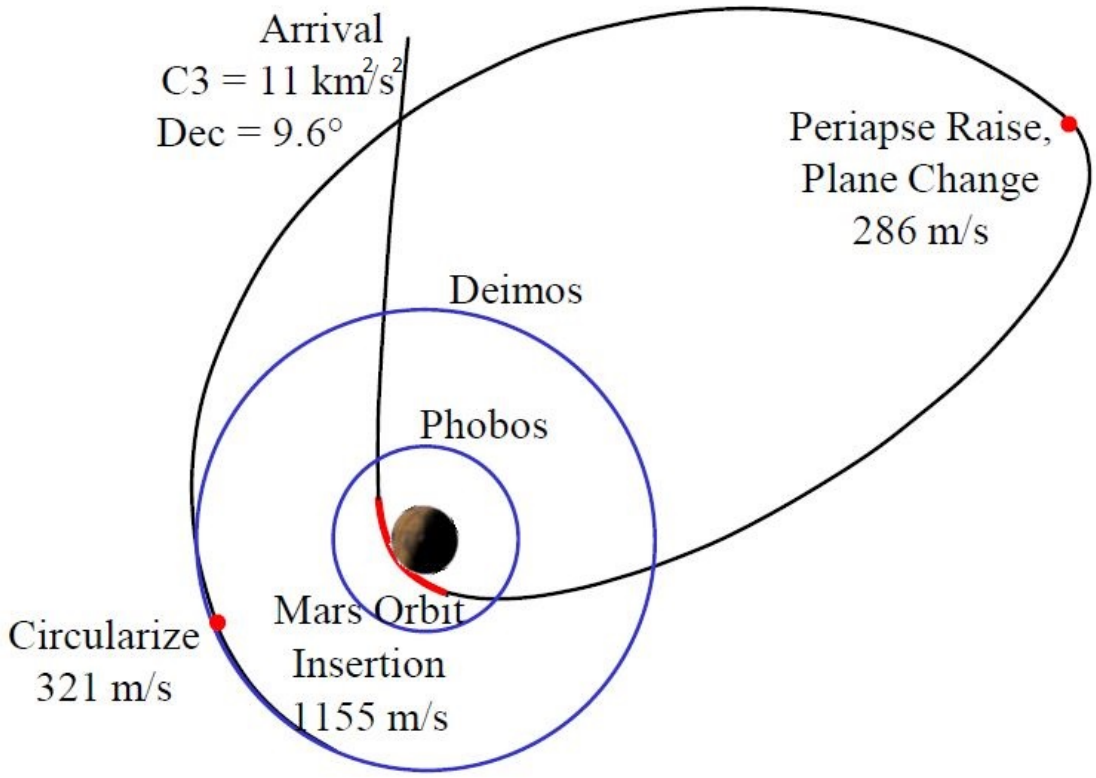

Figure 3 – Three burn bi-elliptic orbit insertion maneuver for rendezvous with Deimos. Source: Hopkins. [5]

In this thesis, a new method of targeting the moons of Mars is developed based on minimizing the maneuvers necessary upon arrival, i.e. within the sphere of influence of Mars. In fact, as stated by Hopkins, using a bi-elliptic maneuver like the example shown in Figure 3 could cause problems:

> "Higher apoapsis altitudes can be used to reduce the delta V somewhat. However, this would increase the duration required to rendezvous with the target moon. Using a very high target apoapsis would mean that a slight propulsion underperformance during orbit insertion would leave the spacecraft in a hyperbolic trajectory, which is a safety concern." [5]

Therefore, it is preferable to have the spacecraft on an arrival trajectory such that upon capture (i.e. after executing a ΔV maneuver to reduce the orbital energy enough to not escape the planet) the spacecraft and desired moon to be targeted are in similar coplanar orbits. In fact, as discussed Chapter 5 in more detail, it is desirable to avoid relatively high inclination ($i > 20°$) arrival orbits with respect to Mars' equatorial plane; indeed, the resulting ΔV to correct for the inclination offset with respect to the moons of Mars is considerably greater than that of an arrival trajectory with small inclination. More details of the arrival scenario presented by Hopkins are discussed and compared with the results obtained in this thesis are reported in Chapter 6.

After the spacecraft is captured and is in a roughly equatorial circular orbit with semi-major axis different than that of the desired targeted moon, a coplanar orbital transfer such as a Hohmann transfer can be executed to rendezvous with the moon and consequently land on it. Although such approach will not be discussed in detail in this thesis, information regarding Phobos or Deimos rendezvous and orbit insertion can be found in *Orbital Operations for Phobos and Deimos Exploration* by Wallace, Parker, Strange, and Grebow. In fact, the gravitational environments of Phobos and Deimos are primarily perturbed by the non-spherical gravity fields of the moons and the strong gravitational effects of Mars.[21] Since the sphere of influence of Phobos and Deimos are below their surface, no direct orbits exist. Instead, it is necessary to analyze the Circular Restricted Three-Body Problem (CR3BP) in the Mars-Phobos and Mars-Deimos systems. The result yields to a series of stable and unstable orbits about the L_1 and L_2 points. Figure 4 shows such results for the Mars-Phobos case. Additionally, "Lagrange-Point orbits require precision navigation and frequent, precise maneuvering" and even a "1 mm/s disturbance causes the spacecraft to depart on the unstable manifold". [21]

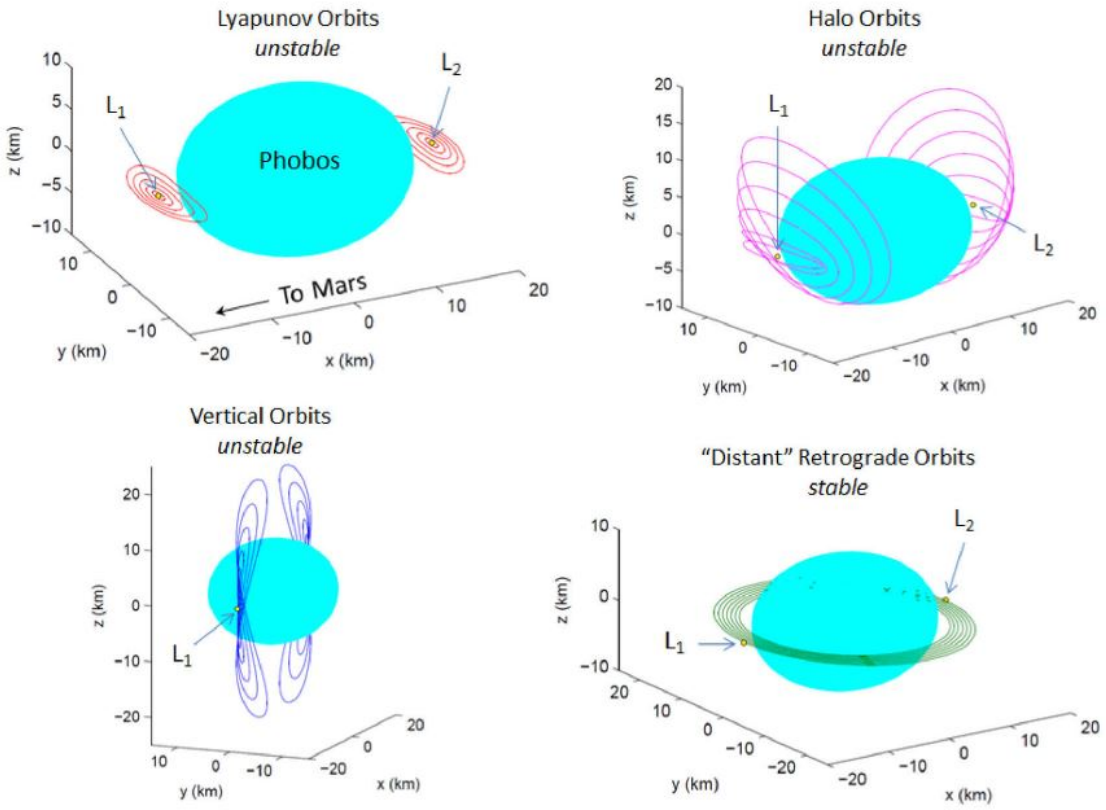

Figure 4 – Periodic orbits in the "ideal model" (CR3BP) of the Mars-Phobos system. Source: Wallace, Parker, Strange, and Grebow, p. 5. [21]

Figure 5 shows more details about an example of a halo orbit[4] about the L_2 point of the Mars-Phobos system. As visible from the altitude graph, the spacecraft gets extremely close to Phobos' surface, about 2 km at its lowest. Due to the highly perturbed environment about Phobos, such low altitude passes could evolve into trajectories that intersect the surface of the Martian moon. Although these cases could be used to land on Phobos, the dynamics of such trajectories are usually unpredictable, especially if a relatively high level of uncertainty in the orbit determination of the spacecraft is present. Consequently, a direct descent and landing on Phobos or Deimos could be the preferable choice for robotic and especially human missions to the moons of Mars.

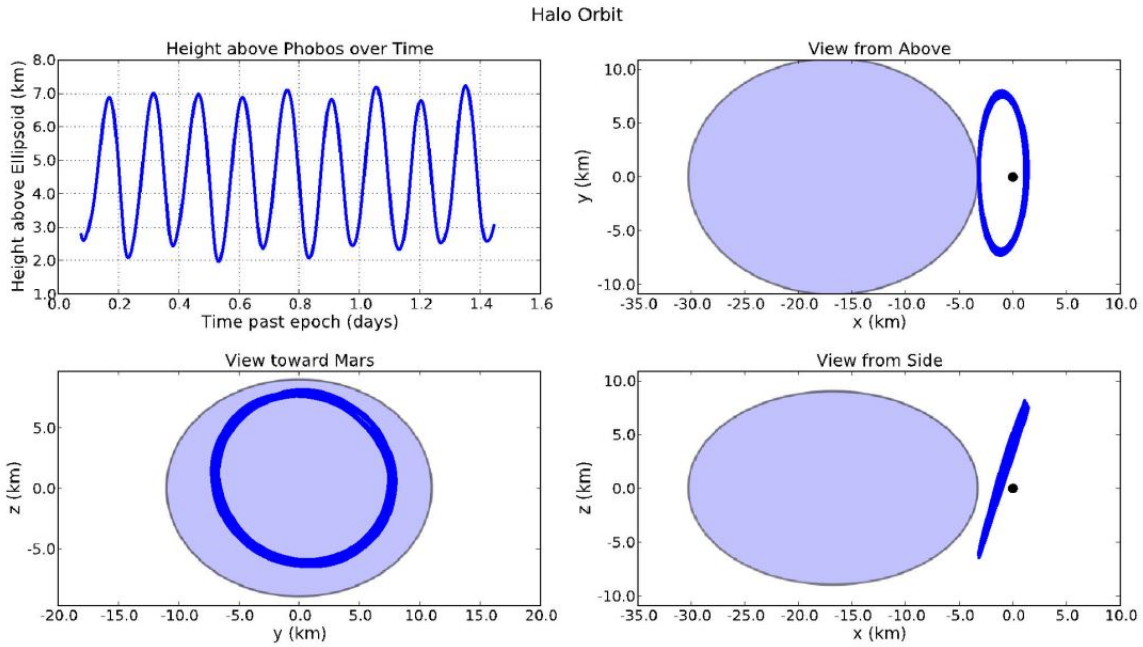

Figure 5 – View of a halo orbit about the L_2 point of the Mars-Phobos system. Source: Wallace, Parker, Strange, and Grebow, p. 7. [21]

Assumptions

The assumptions that were used throughout the analysis of the transfer maneuvers are as follows:

1. All the ΔV maneuvers are treated as impulsive; assuming the use of chemical or nuclear propulsion systems, the burn times required for such ΔVs (in the order of minutes or hours) are considerably much less than the orbital transfer times from Earth to Mars (in the order of months).

2. The only major forces that were considered for the analysis are the point mass gravitational forces of Earth, Mars and the Sun within their respective spheres of influence. Perturbations such as solar radiation pressure, non-uniform gravitational fields, and gravitational effects of other bodies, such as the other planets of the Solar System, were neglected. Therefore, the method of patched conics was used. This method assumes that when a spacecraft is outside

the sphere of influence of a planet, it follows an unperturbed Keplerian orbit (i.e. two-body dynamics) around the Sun. Since interplanetary distances are so vast, for heliocentric orbits it is reasonable to neglect the size of the spheres of influence of Earth and Mars, and consider them to be just points in space coinciding with the planetary centers. Additionally, within each planet's sphere of influence, the spacecraft travels an unperturbed Keplerian path about the planet. While the sphere of influence appears small on the scale of the solar system, from the point of view of the planet it is "large enough" to be considered to extend to infinity.

3. Phobos and Deimos are both in circular equatorial orbits about Mars. As shown in Table 1, the actual values of inclination and eccentricity of the moons are not zero, but are considerably small and therefore negligible for the analysis conducted in this thesis.

Table 1 – Key orbital parameters of the Martian moons Phobos and Deimos.[23]

Key Orbital Parameters of Phobos and Deimos			
	Eccentricity	Inclination (deg)*	Semi-major Axis (km)
Phobos	0.0151	1.08	9378
Deimos	0.0005	1.79	23459

*Value measured with respect to the Martian equatorial plane.

MATLAB

MATLAB® is a high-level language and interactive environment for numerical computation, visualization, and programming. [13] MATLAB was used in this research to implement the necessary algorithms into computer codes as shown in the flowcharts of Appendix A and Appendix B. Additionally, Appendix C presents information on computing time considerations. All the graphical results shown in this thesis were obtained by running the appropriate MATLAB scripts.

Lambert's Problem

Most of the analysis conducted in this thesis is based on the formulation and solution of a problem in the field of astrodynamics that the Swiss mathematician Johann Heinrich Lambert (1728 – 1779) formulated in 1761[10]. This problem is now known as Lambert's problem. In spacecraft targeting applications, it is essential to know the time of flight required to travel a particular trajectory. In fact, as discussed in greater details in Chapter 3, Lambert's problem is a boundary value problem involving two position vectors and a time of flight between them. Additionally, according to Lambert's conjecture, only these three parameters, two position vectors and time of flight, are necessary to uniquely define an orbital transfer between the two points. From the solution to Lambert's problem it is then possible to calculate the required ΔVs.

In the case of an Earth-Mars transfer, the first step required to set up Lambert's problem is being able to identify Earth's and Mars' positions for given departure and arrival dates. Chapter 2 discusses how to obtain the position and velocity vectors of the two planets as a function of time. Moreover, the solution to Lambert's problem is used in combination to other constraints to determine the orientation and shape of the arrival hyperbolic trajectory about Mars.

Chapter 2

Determining Position and Velocity Vectors of Earth and Mars for a Given Date

In order to analyze possible transfer orbits from Earth to Mars it is necessary to obtain the position and velocity vectors of the planets at the desired departure and arrival dates. Various methods to do so exist, but in this thesis only two main methods are considered: Standish's algorithm[19] and JPL HORIZONS[7]. Note that the orbital position and velocity of Earth and Mars are described by three-dimensional vectors although the transfer orbit between the two planets is a two-dimensional transfer. In fact, the orbital transfer defines a plane on which the Sun, the Earth at departure and Mars at arrival lie on.

Position Vectors of Earth and Mars

Determining the position and velocity vectors of Earth and Mars can be done using the results presented in Standish. Here, a detailed algorithm of how to determine the position of the eight planets (Mercury through Neptune) and Pluto for a given date is offered. Note that such dates must be inputted as Julian Ephemeris Dates. To convert dates from the day/month/year format to Julian Dates, Algorithm 14 taken from Vallado, p.189[20] is used. Additionally, it must be noted that Standish's algorithm provides approximate positions for the planets. This method should not be used unless its errors are acceptable for the application taken into account. High precision ephemerides for the planets are available via the JPL HORIZONS system. The analysis and the following results presented in this thesis are based on the accuracy of Standish's algorithm, although a comparison with the HORIZONS system was also done.

Once the position vectors of Earth and Mars are obtained, both vectors are converted into the same inertial reference frame. For simplicity and convenience, the J2000 ecliptic plane was used. By definition, this plane contains both the Sun and Earth. Additionally, this reference frame is defined by having the x-axis aligned with Earth's vernal equinox, the z-axis pointing normal to the ecliptic plane, while the y-axis completes the right-handed coordinate system, as shown in Figure 2. Moreover, the z-position of Earth with respect to the Sun is exactly zero on January 1, 2000. Standish's algorithm makes use of the J2000 ecliptic plane as described above. The reference frame in which HORIZONS works can be chosen from a set of predefined reference frames, and it was set to the J2000 ecliptic reference frame for the following applications.

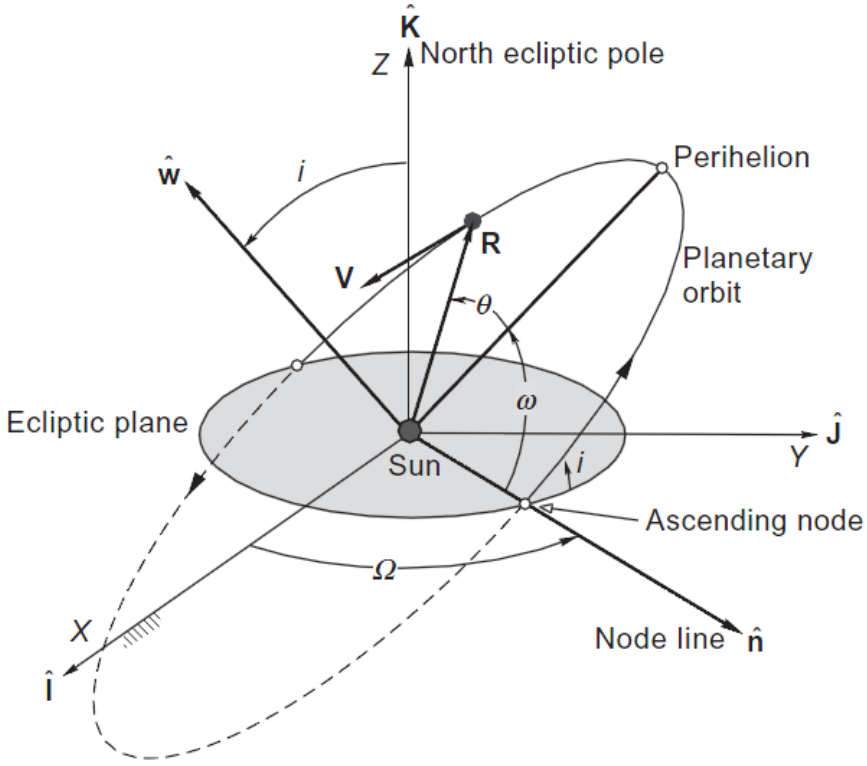

Figure 6 – Planetary orbit in heliocentric ecliptic frame; in the figure, R and V are respectively the position and the velocity vectors of the planet taken into consideration. Source: Curtis, p. 471.[2]

For example, consider an arbitrary date, say January 22, 2014 at 00:00:00.0 (UT). The position vectors of Earth and Mars in J2000 ecliptic reference frame are given as shown in Table 2. Comparing the results obtained by using Standish's algorithm with those of JPL HORIZONS, it can be noted that the difference is relatively small. In fact, for the purpose of the analysis done in this thesis, the results obtained using Standish's algorithm are sufficient. Additionally, note that the position vector of a planet can be expressed as:

$$\vec{r}^{E} = r_x \hat{I} + r_y \hat{J} + r_z \hat{K} \tag{1}$$

where $\hat{I}, \hat{J}, \hat{K}$ are the unit vectors that define the J2000 ecliptic coordinate frame, 'E'.

Table 2 – Comparison between position vectors of Earth and Mars using Standish's algorithm and using JPL HORIZONS; note that the z-component is considerably smaller than the x and y components.

Earth's Position (AU) on January 22, 2014 at 00:00:00.0 (UT)			
	r_x	r_y	r_z
Standish's algorithm	-0.51686	0.83751	-0.000026827
JPL HORIZONS	-0.51570	0.83531	-0.000120055
Mars' Position (AU) on January 22, 2014 at 00:00:00.0 (UT)			
	r_x	r_y	r_z
Standish's algorithm	-1.60258	0.44615	0.048689
JPL HORIZONS	-1.60145	0.44411	0.048592

Additionally, using either method for calculating the position vectors of the planets, the eccentric anomaly can be found. Note that both methods assume that, unlike for the standard two-body problem, the orbital elements of the planets' orbits change in time. Even though such changes are minimal and become more noticeable in an interval of time of the order of centuries, they were still taken into account in the analysis that follows.

Velocity Vectors of Earth and Mars

Once the position vectors of the planets are found, it is necessary to compute the velocity vectors. First, velocity vectors in perifocal coordinates are calculated. As Figure 7 shows, the perifocal coordinate reference frame is defined with the center being the focus (in this case the Sun); by the $\hat{p}$-coordinate pointing in the direction of the planet's periapse location, by the $\hat{w}$-coordinate pointing normal to the orbital plane such that the planet's motion is counterclockwise and by the $\hat{q}$-coordinate which completes the right-handed reference frame. Additionally, $\bar{x}$ and $\bar{y}$ are the components of the distance of the planet from the Sun in the $\hat{p}$-direction and $\hat{q}$-direction respectively; hence, by using the Pythagorean Theorem, $r = \sqrt{\bar{x}^2 + \bar{y}^2}$ results in the magnitude of the radius from the center of the central body.

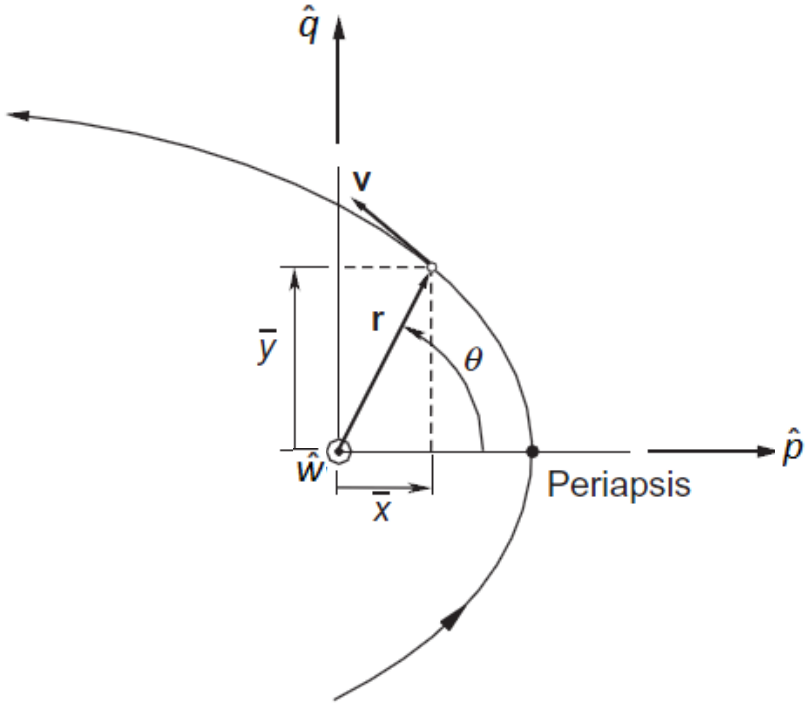

Figure 7 – Position and velocity relative to the $\hat{p}\hat{q}\hat{w}$ perifocal reference frame. Source: Curtis, p. 114.[7]

Successively, a direction cosine matrix can be used to obtain the velocity vectors in J2000 coordinate frame. In perifocal coordinates, the velocity vector of a planet orbiting the Sun is defined as follows:

$$\vec{v}^P = -\sqrt{\frac{\mu_{Sun}}{p}}\sin\theta\ \hat{p} + \sqrt{\frac{\mu_{Sun}}{p}}(e + \cos\theta)\hat{q} \tag{2}$$

While μ_{Sun} and e are known, p and θ must be calculated. Given eccentric anomaly E, which was obtained through Standish's algorithm, and knowing the semi-major axis a, the true anomaly θ and semi-latus rectum p can be calculated:

$$\theta = 2\tan^{-1}\left[\sqrt{\frac{1+e}{1-e}}\tan\left(\frac{E}{2}\right)\right] \tag{3}$$

$$p = a\,(1 - e^2) \tag{4}$$

The direction cosine matrix (DCM) used to convert $\vec{v}^P$ into $\vec{v}^E$ such that $\vec{v}^E = C^{PE}\vec{v}^P$ is given by:

$$C^{PE} = \begin{bmatrix} \cos\Omega\cos\omega - \sin\Omega\sin\omega\cos i & -\cos\Omega\sin\omega - \sin\Omega\cos\omega\cos i & \sin\Omega\sin i \\ \sin\Omega\cos\omega + \cos\Omega\sin\omega\cos i & -\sin\Omega\sin\omega + \cos\Omega\cos\omega\cos i & -\cos\Omega\sin i \\ \sin\omega\sin i & \cos\omega\sin i & \cos i \end{bmatrix} \tag{5}$$

Note that once the perifocal frame is determined, Eq. (5) is the DCM used to convert from perifocal to J2000 ecliptic reference frame. Therefore, the velocity vectors can now be rewritten in the J2000 ecliptic reference frame as:

$$\vec{v}^E = v_x\hat{I} + v_y\hat{J} + v_z\hat{K} \tag{6}$$

Table 3 shows a comparison between the velocity x,y, and z components obtained using Standish's algorithm and those obtained from JPL HORIZONS.

Table 3 - Comparison between velocity vectors of Earth and Mars using Standish's algorithm and using JPL HORIZONS; note that the z-component is considerably smaller than the x and y components.

Earth's Velocity (km/s) on January 22, 2014 at 00:00:00.0 (UT)			
	v_x	v_y	v_z
Standish's algorithm	-25.8345	-15.7563	-0.00050470
JPL HORIZONS	-25.8265	-15.7390	-0.00066392
Mars' Velocity (km/s) on January 22, 2014 at 00:00:00.0 (UT)			
	v_x	v_y	v_z
Standish's algorithm	-5.59172	-21.2728	-0.50470
JPL HORIZONS	-5.58394	-21.2665	-0.30861

Given a departure date from Earth and an arrival date at Mars, it is the possible to determine what the planets' position and velocities would be on those days. This information will be used to solve Lambert's problem as explained in the following chapter.

Chapter 3

Lambert's Problem

In order to determine the transfer trajectory orbital parameters and the necessary ΔVs to accomplish such transfer, it is essential to solve Lambert's Problem. In astrodynamics, Lambert's problem is a two-point boundary value problem (see Figure 8) for the following governing equation of motion:

$$\ddot{\vec{r}} = -\frac{\mu \vec{r}}{r^3} \tag{7}$$

In the case of an Earth to Mars transfer, the boundary conditions become:

$$\vec{r}_1(t_1) = \vec{r}\left(t_{departure}\right) = \vec{r}_{Earth} \tag{8}$$

$$\vec{r}_2(t_2) = \vec{r}(t_{arrival}) = \vec{r}_{Mars} \tag{9}$$

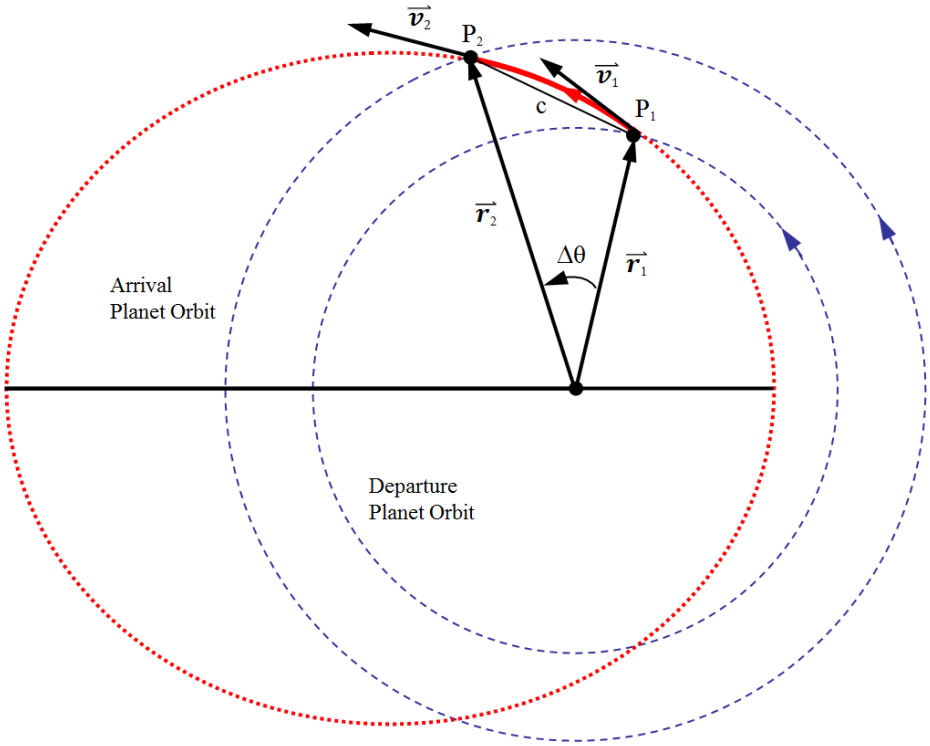

Figure 8 – Geometry of Lambert problem for an interplanetary trajectory.

The innovative conjecture Lambert had developed is based on geometric reasoning. In fact, Lambert believed that the time required to traverse an elliptic arc between two points depends only on the size of the orbit, i.e. semimajor axis a, on the chord length c and the sum of the radii from the focus to points P_1 and P_2, or $r_1 + r_2$. Mathematically, this can be expressed as follows:

$$t_2 - t_1 = f(a, c, r_1 + r_2) \tag{10}$$

Starting from Kepler's equation, Eq. (11), it is possible to derive Lambert's equation, Eq. (12), such that it does not depend on eccentricity. Such derivation can be found in most astrodynamics textbooks such as Prussing and Conway, pages 67-70. [10]

$$E_2 - E_1 - e(\sin E_2 - \sin E_1) = \sqrt{\frac{\mu}{a^3}}(t_2 - t_1) \tag{11}$$

$$a^{3/2}[\alpha - \sin\alpha - (\beta - \sin\beta)] = \sqrt{\mu}(t_2 - t_1) \tag{12}$$

In Eq. (12), the unknown to solve for is semi-major axis a while α and β are defined as:

$$\sin\left(\frac{\alpha}{2}\right) = \left(\frac{s}{2a}\right)^{1/2} \tag{13}$$

$$\sin\left(\frac{\beta}{2}\right) = \left(\frac{s-c}{2a}\right)^{1/2} \tag{14}$$

$$s = \frac{1}{2}(r_1 + r_2 + c) \tag{15}$$

$$c = \sqrt{{r_1}^2 + {r_2}^2 - r_1 r_2 \cos\Delta\theta} \tag{16}$$

$$\Delta\theta = \begin{cases} \cos^{-1}\left(\frac{\vec{r}_1 \cdot \vec{r}_2}{r_1 r_2}\right) & if\ \left[(\vec{r}_1 x\, \vec{r}_2)\cdot\hat{K}\right] \geq 0 \\ 2\pi - \cos^{-1}\left(\frac{\vec{r}_1 \cdot \vec{r}_2}{r_1 r_2}\right) & if\ \left[(\vec{r}_1 x\, \vec{r}_2)\cdot\hat{K}\right] < 0 \end{cases} \tag{17}$$

Note that, given the definitions of α, β and s, it can be seen that, as expected, Eq. (12) depends only on a, c, and $r_1 + r_2$.

Derivation of Lambert's Problem Solution Using the Universal Variable

The solution to Lambert's Problem gives the departure and arrival velocity vectors, $\vec{v}_1$ and $\vec{v}_2$ in Figure 8, that an arbitrary spacecraft needs to achieve in order to perform the transfer trajectory from P_1 to P_2 for a given amount of time. In this analysis, Lambert's Problem was applied to the heliocentric cruise neglecting the sizes of the departure and arrival planets' spheres of influence. Additionally, only prograde orbital transfers were considered.

In order to obtain $\vec{v}_1$ and $\vec{v}_2$ in the J2000 ecliptic reference frame, Langrange coefficients can be used. In fact, starting from the general relationship involving Lagrange coefficients f, $\dot{f}$, g, $\dot{g}$

$$\begin{Bmatrix} \vec{r}_2 \\ \vec{v}_2 \end{Bmatrix} = \begin{bmatrix} f & g \\ \dot{f} & \dot{g} \end{bmatrix} \begin{Bmatrix} \vec{r}_1 \\ \vec{v}_1 \end{Bmatrix} \tag{18}$$

the velocities $\vec{v}_1$ and $\vec{v}_2$ can be expressed as functions of the boundary conditions (i.e. the position vectors $\vec{r}_1$ and $\vec{r}_2$) as follows:

$$\vec{v}_1 = \frac{1}{g}(\vec{r}_2 - f\vec{r}_1) \tag{19}$$

$$\vec{v}_2 = \frac{1}{g}(\dot{g}\vec{r}_2 - \vec{r}_1) \tag{20}$$

The Lagrange coefficients can be found using the following relationships. Note that $\vec{v}_1$ and $\vec{v}_2$ do not involve $\dot{f}$. Hence, $\dot{f}$ was not taken into account.

$$f = 1 - \frac{y(z)}{r_1} \tag{21}$$

$$g = A\sqrt{\frac{y(z)}{\mu}} \tag{22}$$

$$\dot{g} = 1 - \frac{y(z)}{r_2} \tag{23}$$

$$A = \pm \sin\Delta\theta \sqrt{\frac{r_1 r_2}{1-\cos\Delta\theta}} \tag{24}$$

$$y(z) = r_1 + r_2 + A\frac{zC_3(z)-1}{\sqrt{C_2(z)}} \tag{25}$$

The sign of A in Eq. (24) is assessed in the next section. In Eq. (25), $C_3(z)$ and $C_2(z)$ are Stumpff functions and are defined by the following expressions:

$$C_2(z) = \begin{cases} \frac{1-\cos\sqrt{z}}{z} & if\ z > 0 \\ \frac{\cosh\sqrt{-z}-1}{-z} & if\ z < 0 \\ \frac{1}{2} & if\ z = 0 \end{cases} \tag{26}$$

$$C_3(z) = \begin{cases} \frac{\sqrt{z}-\sin\sqrt{z}}{z^{3/2}} & if\ z > 0 \\ \frac{\sin\sqrt{-z}-\sqrt{-z}}{(-z)^{3/2}} & if\ z < 0 \\ \frac{1}{6} & if\ z = 0 \end{cases} \tag{27}$$

Moreover, z is a variable defined as

$$z = \tilde{\alpha}\chi^2 \tag{28}$$

$$\tilde{\alpha} = \frac{1}{a} \tag{29}$$

In order to solve for the value of z, it is necessary to find the zeroes of the following transcendental function:

$$F(z) = \left[\frac{y(z)}{C_2(z)}\right]^{3/2} C_3(z) + A\sqrt{y(z)} - \sqrt{\mu}(t_2 - t_1) \tag{30}$$

i.e. solving the equation $F(z) = 0$, which can be done by using a root finding method such as the Newton-Raphson method. Once a guess on the initial value of z is made, then the following equation can be solved iteratively until a certain relative tolerance is satisfied:

$$z_{i+1} = z_i - F(z_i)/F'(z_i) \tag{31}$$

Here, $F'(z_i) = \frac{\partial F(z_i)}{\partial z_i}$. Note that a good initial guess for z would be $z = 0$. Additionally, in Eq. (28) χ is known as the universal anomaly. Using χ when solving Lambert's problem is preferable because it avoids encountering discontinuities when iterating to solve for z. In fact, the solution to Lambert's problem can yield an elliptical or hyperbolic transfer trajectory, depending on the given departure and arrival times. Because of this fact, while iterating to solve for z, the value of

semimajor axis a could vary between positive, negative, and undefined. If "regular variables" instead of the universal variable were to be used, this latter possible value that a could attain would cause the iterative process for finding z to be inconclusive. Therefore, no solution for the Lambert's Problem would be found.

Once the value of z is determined within a certain tolerance, then the velocity vectors $\vec{v}_1$ and $\vec{v}_2$ can be computed using the Lagrange coefficients as mentioned previously. The next sections present a special case of the minimal energy Lambert's Problem solution and a summarized step-by-step algorithm for solving the Lambert's Problem.

Minimum Energy Solution

In order to resolve the sign of Eq. (24), the minimum energy transfer must be assessed. In fact, the minimum transfer energy for the Lambert's solution happens when the characteristic orbital energy $\varepsilon = -\frac{\mu}{2a}$ is minimum. It can be shown that ε is minimized when

$$a_m = \frac{s}{2} \tag{32}$$

Note that the subscript *m* stands for "minimum." Substituting Eq. (32) into Eq. (13) and solving for α yields to $\alpha_m = \pi$. Using this value for α_m in Eq. (14) and solving for β results in $\beta_m = 2\sin^{-1}\sqrt{\frac{s-c}{s}}$. Using α_m and β_m in Eq. (12) permits to solve for $(t_2 - t_1)_m$:

$$\Delta t_m = (t_2 - t_1)_m = \frac{1}{\sqrt{\mu}}\left(\frac{s^3}{8}\right)^{\frac{1}{2}}(\pi - \beta_m + \sin\beta_m) \tag{33}$$

Note that minimizing the energy of the transfer orbit does not result in the minimum time of flight. Additionally, the values for semilatus rectum and eccentricity of the minimum energy transfer can be determined as follows:

$$p_m = \frac{r_1 r_2(1-\cos\Delta\theta)}{c} \tag{34}$$

$$e_m = \sqrt{1 - \frac{p_m}{a_m}} \tag{35}$$

Once the value of Δt_m is determined, then for a given time of flight $(t_2 - t_1)$, A from Eq. (24) can be determined as follows:

$$A = \begin{cases} \sin\Delta\theta \sqrt{\frac{r_1 r_2}{1-\cos\Delta\theta}} & if\ \Delta t_m \geq (t_2 - t_1) \\ -\sin\Delta\theta \sqrt{\frac{r_1 r_2}{1-\cos\Delta\theta}} & if\ \Delta t_m < (t_2 - t_1) \end{cases} \tag{36}$$

Algorithm for Solving Lambert's Problem

This section illustrates a step-by-step algorithm to solve the general case of the Lambert's Problem for an interplanetary transfer from Earth to Mars. Prograde motion is assumed for all possible transfer orbits. Appendix A comprises of a flowchart that illustrates how this algorithm can be implemented in a computer language such as MATLAB in order to make computations such as the iterative process to find z faster.

Solution to Lambert's Problems for given departure and arrival dates:

1. t_{dep} and t_{arr} are given
2. Compute $\vec{r}_{Earth}$, $\vec{r}_{Mars}$, using the method described in Chapter 2.
3. Find the values of $|\vec{r}_{Earth}|$, $|\vec{r}_{Mars}|$ (lengths of the position vectors), chord c, transfer angle $\Delta\theta$, s and A
4. Iterate to get the value of z
5. Solve for $y(z)$
6. Find the Lagrange coefficients: f, g, $\dot{g}$
7. Compute $\vec{v}_1$ and $\vec{v}_2$

Planetary Departure

Once $\vec{v}_1$ and $\vec{v}_2$ are determined via the solution to Lambert's Problem, planetary departure and arrival must be considered. In fact, when setting up Lambert's Problem, the spheres of influence of Earth and Mars were ignored. In reality, before being able to leave Earth's sphere of influence, it is necessary to transit from a parking elliptical orbit about Earth to a hyperbolic orbit as shown in Figure 9.

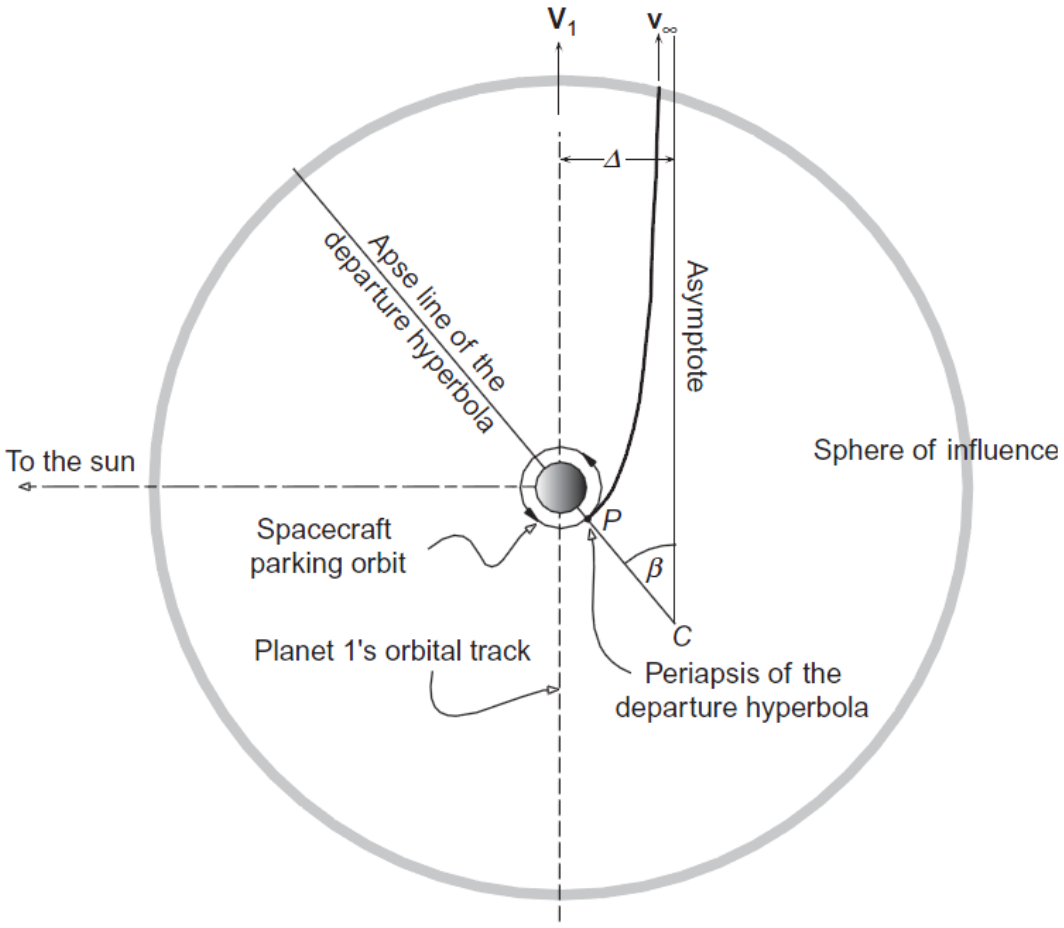

Figure 9 – Departure orbit geometry. Source: Curtis, p. 443.[2]

Hence, the velocity of the spacecraft's hyperbolic orbit at the boundary of the sphere of influence with respect to Earth must be:

$$\vec{v}_{\infty/Earth} = \vec{v}_{sc/Sun,1} - \vec{v}_{Earth/Sun} \tag{37}$$

Here, $\vec{v}_{sc/Sun,1} = \vec{v}_1$ which was calculated from the Lambert's Problem while $\vec{v}_{Earth/Sun} = \vec{v}_{Earth}$ which is the velocity of Earth with respect to the Sun. The latter quantity can be obtained from Standish's algorithm as explained in Chapter 2. Therefore, it is possible to compute $\vec{v}_{\infty/Earth}$ and its magnitude. Additionally, note that Eq. (37) is a vector relation and therefore comparing the various velocity magnitudes does not suffice and is only applicable when all vectors are parallel to each other.

In order to determine the necessary Δv to put the spacecraft onto a hyperbolic trajectory, initial orbital conditions of the spacecraft parking orbit must be given as shown on Figure 9. Assuming a circular parking orbit around the Earth with known altitude h_{Earth}, the velocity of the spacecraft can be calculated as follows:

$$v_{c,Earth} = \sqrt{\frac{\mu_{Earth}}{R_{Earth}+h_{Earth}}} \tag{38}$$

Then, using the vis-viva equation, it is possible to write an energy balance between the parking orbit and the hyperbolic orbit:

$$\frac{\left(v_{\infty/Earth}\right)^2}{2} = \frac{\left(v_{c,Earth}+\Delta v_1\right)^2}{2} - \frac{\mu_{Earth}}{R_{Earth}+h_{Earth}} \tag{39}$$

In Eq. (39) the only unknown is Δv_1. Solving for Δv_1 yields to two different solutions only one of which is positive and is hence the correct answer. Usually, the term $\left(v_{\infty/Earth}\right)^2$ is referred to as $C3$. More generally,

$$C3 = \left(v_{\infty/Departure\ Planet}\right)^2 \tag{40}$$

$C3$ is therefore related to the characteristic energy of the departure hyperbolic orbit. Additionally, $C3$ is a key parameter used in interplanetary trajectory design as discussed in Chapter 4.

Planetary Arrival

After the spacecraft travels from Earth to the sphere of influence of Mars, another maneuver must be performed in order to have the spacecraft be captured by the arrival planet. In fact, as Figure 10 shows, if no Δv_2 is executed the spacecraft would do a flyby of Mars without entering a closed elliptical orbit around it and leaving its sphere of influence on a flyby trajectory.

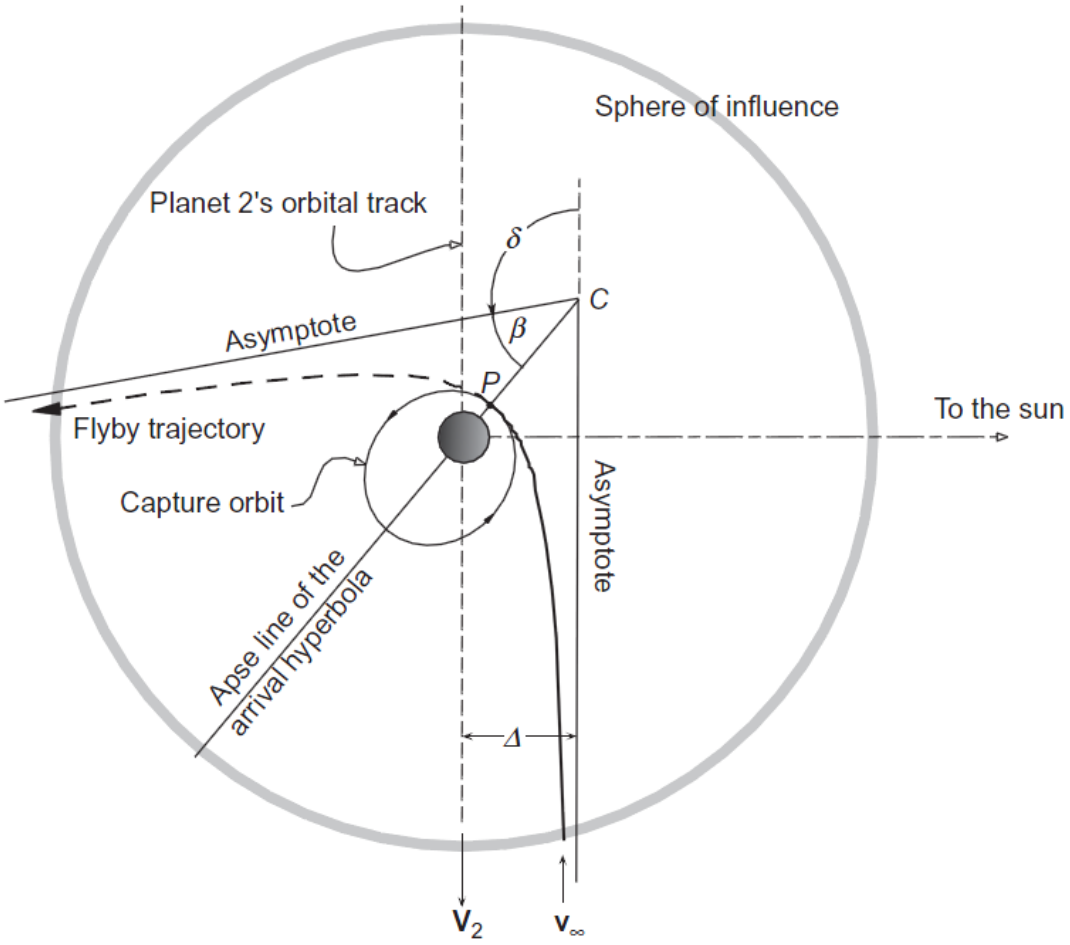

Figure 10 – Planetary approach. Source: Curtis, p. 451.[2]

From the solution to Lambert's Problem, it is possible to obtain $\vec{v}_{\infty/Mars}$ as follows:

$$\vec{v}_{\infty/Mars} = \vec{v}_{sc/Sun,2} - \vec{v}_{Mars/Sun} \tag{41}$$

Similarly to the previous section, $\vec{v}_{sc/Sun,2} = \vec{v}_2$ and $\vec{v}_{Mars/Sun}$ can be computed with the method described in Chapter 2. Thus, after computing $\vec{v}_{\infty/Mars}$ using Eq. (41), it is possible to solve for Δv_2 from the following equation:

$$\frac{(v_{\infty/Mars})^2}{2} = \frac{(v_{c,Mars}+\Delta v_2)^2}{2} - \frac{\mu_{Mars}}{R_{Mars}+h_{Mars}} \tag{42}$$

Note that the above expression is true for a Δv_2 performed at the hyperbolic periapse which corresponds to the desired final spacecraft parking orbit altitude, h_{Mars}. Additionally, $v_{c,Mars}$ can be calculated as follows:

$$v_{c,Mars} = \sqrt{\frac{\mu_{Mars}}{R_{Mars}+h_{Mars}}} \tag{43}$$

In the approach section of the spacecraft journey from Earth to Mars, it should be noted that the main design parameter upon which the rest of a mission is constructed on is $v_{\infty/Mars}$.

Sphere of Influence Considerations

As mentioned in Chapter 1, the spheres of influence of Earth and Mars are considered to be relatively small for the heliocentric transfer and relatively large for the planetary departure and arrival. The formula for computing the radius of the sphere of influence r_{SOI} of a planet in the Solar System is given by:

$$r_{SOI} \approx r_{planet}\left(\frac{\mu_{planet}}{\mu_{Sun}}\right)^{2/5} \tag{44}$$

Here, r_{planet} is the semimajor axis of the planet's orbit around the Sun. A derivation of Eq. (44) can be found in Wiesel on p. 320-322. When calculating r_{SOI} for Earth and Mars, it can be found that:

$$r_{SOI,Earth} \approx 924{,}652\ km\ or\ 145\ body\ radii$$

$$r_{SOI,Mars} \approx 577{,}133\ km\ or\ 170\ body\ radii$$

Hence, the assumptions made about the spheres of influence of Earth and Mars hold, especially if considering the energy balance expression for a hyperbolic to elliptic transfer, or vice-versa:

$$\frac{\left(\vec{v}_{\infty/Planet}\right)^2}{2} - \frac{\mu_{Planet}}{r_{SOI}} = \frac{\left(v_{c,Planet}+\Delta v\right)^2}{2} - \frac{\mu_{Planet}}{R_{Planet}+h_{Planet}} \tag{45}$$

In Eq. (45) it can be noted that the term $-\frac{\mu_{Planet}}{r_{SOI}} \to 0$ as $r_{SOI} \to \infty$ or, for more practical applications, as r_{SOI} becomes large enough. Thus, Eq. (45) can be simplified to:

$$\frac{\left(\vec{v}_{\infty/Planet}\right)^2}{2} = \frac{\left(v_{c,Planet}+\Delta v\right)^2}{2} - \frac{\mu_{Planet}}{R_{Planet}+h_{Planet}} \tag{46}$$

Total ΔV Calculation and Propellant Mass

In order to obtain the total Δv the overall Earth-Mars transfer requires, one can compute such quantity as follows:

$$\Delta v_{tot} = \Delta v_1 + \Delta v_2 \tag{47}$$

Note that Δv_{tot} does not usually represent the total Δv budget for a mission. In fact, other minor maneuvers such as trajectory correction maneuvers were not taken into account in this analysis. Another key mission parameter is represented by propellant mass. A quick estimate of how much propellant is needed for given mission and propulsion system is given by:

$$m_p = m_1\left(1 - e^{-\Delta v_{tot}/v_{ex}}\right) \tag{48}$$

Here, m_1 represents the initial mass of the spacecraft (payload, structure, and propellant) while v_{ex} is the exhaust velocity of the propulsion system, or:

$$v_{ex} = I_{sp} * g_{SL} \tag{49}$$

where g_{SL} is the acceleration due to gravity at sea level on Earth. Without knowing the total mass of the spacecraft, it is still possible to rearrange Eq. (48) and solve for propellant mass as a percentage of the total mass:

$$\left(\frac{m_p}{m_1}\right)_{percentage} = \left(1 - e^{-\frac{\Delta v_{tot}}{v_{ex}}}\right) * 100\% \quad (50)$$

Examples of Δv and $\left(\frac{m_p}{m_1}\right)_{percentage}$ for a give set of departure and arrival dates are given in Chapter 4.

Chapter 4

Porkchop Plots

Porkchop plots are computer-generated contour plots that display launch dates vs. arrival dates for characteristics of an interplanetary flight path for a given launch and arrival opportunity between two planets within the Solar System[15]. Perhaps the most important characteristics of porkchop plots are $C3$ at departure (or $CL3$) and v_∞ at arrival. In fact, by looking at a porkchop plot it is possible to choose the launch and arrival windows given specific spacecraft performance such as Δv and I_{sp}. Figure 11 shows an example of a porkchop plot where contour lines of constant $C3$ and arrival v_∞ are displayed in red and blue respectively. Additionally, lines of constant time of flight are shown in green. Porkchop plots can be obtained by solving Lambert's Problem for all the possible combination of departure vs. arrival dates provided that no arrival date is earlier than any departure date. Because such task is computationally time consuming, using a computer program such as MATLAB is essential. A flowchart in Appendix B shows how the solution to the Lambert's Problem algorithm presented in Chapter 3 can be expanded in order to create porkchop plots.

Considering the porkchop plot of Figure 6, one can pick departure and arrival dates, say July 30, 2020 and February 5, 2021 respectively, to determine some of the key parameters of the resulting orbital transfer. The two dates (the two dotted lines in Figure 6) define a specific point on the graph which, for convenience, was denoted by an orange dot. From the graph, it is visible that the orange dot lies close to the contour line corresponding to $C3L \approx 14\ km^2/s^2$ and the contour line corresponding to the arrival $v_\infty \approx 2.7\ km/s$. Additionally, it is possible to estimate the time of flight to be about 190 days since the dot lies slightly below 200-day TOF (green line).

In other words, for this 190 day transfer a characteristic energy of about 14 km^2/s^2 must be reached by the spacecraft as it is leaving Earth's sphere of influence; also, upon arrival to Mars, the spacecraft would enter Mars' sphere of influence with a speed of approximately 2.7 km/s. Note that in order to know more accurate results for $C3L$, v_∞ and time of flight, it is necessary to consult the numerical results that MATLAB gives.

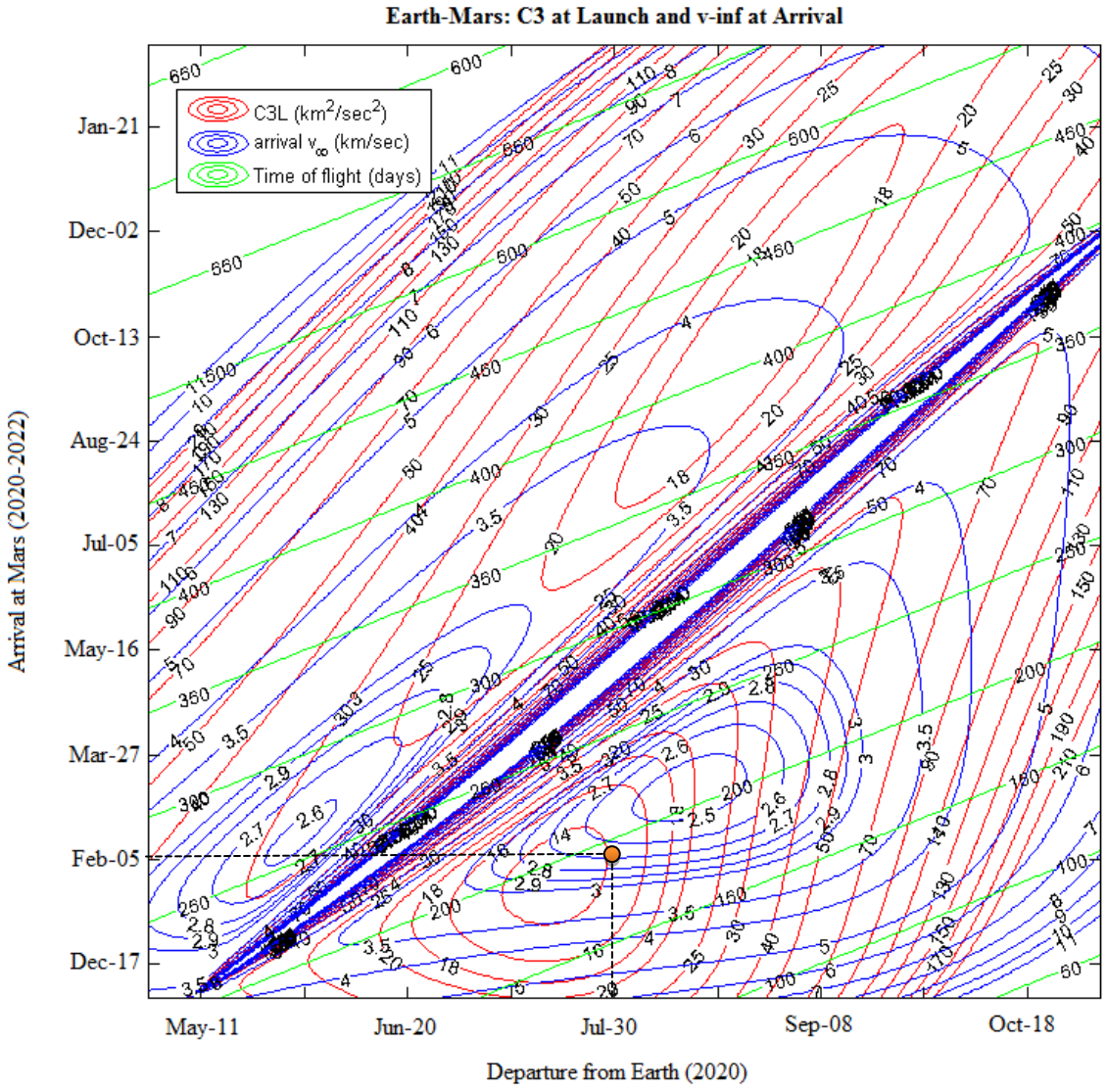

Figure 11 – Porkchop plot for the years 2020-2022 timeframe. The orange dot represents the sample point used in this section to explain how to read a porkchop plot.

Key Features of a Porkchop Plot

One of the key features of porkchop plots is the presence of a singularity shown on the plot as a diagonal line usually going from the bottom left corner to the upper right corner where the values of $C3$ and arrival v_∞ get extremely large. This singularity is due to the fact that 0 and, most importantly, 180 degree transfers (i.e. $\Delta\theta = 0°$ and $\Delta\theta = 180°$) make the transfer plane between departure and arrival undefined as explained in Chapter 6. Because of this fact, solutions of Lambert's Problem close to the singularity give unpractical results for interplanetary trajectory design. Additionally, this singularity divides the possible transfer orbits into two main classes: type I transfers and type II transfers. The former are defined for having $0° < \Delta\theta < 180°$ and are found in the region bounded above by the singularity diagonal; the latter are defined for having $180° < \Delta\theta < 360°$ and are found in the region bounded below by the singularity diagonal. Examples of type I and type II transfers are shown in Figure 12 and Figure 13 respectively. Note that in these figures blue, red and green represent Earth's orbit, Mars' orbit, and the transfer orbit Earth-Mars respectively.

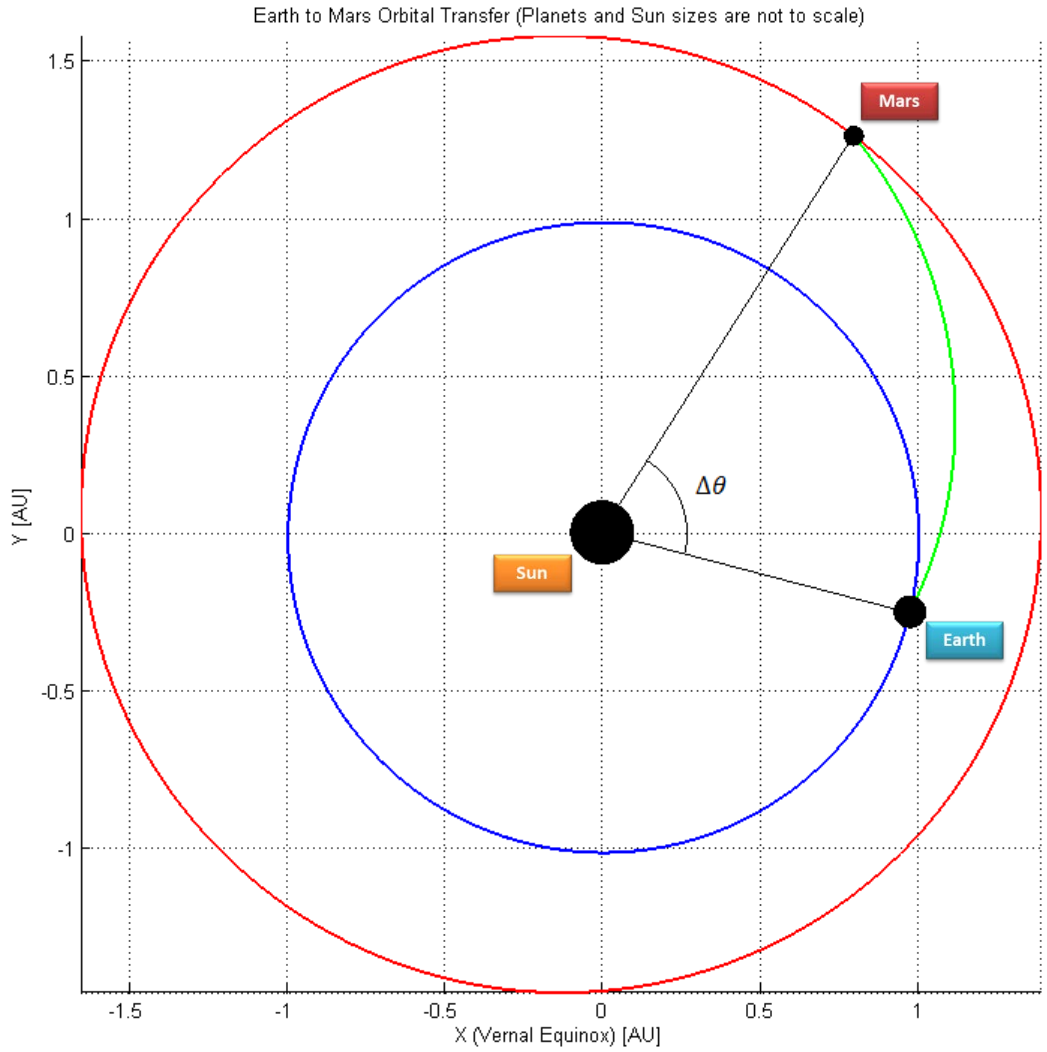

Figure 12 – Example of a Type I transfer with launch on September 8, 2020 and arrival on December 17, 2020.

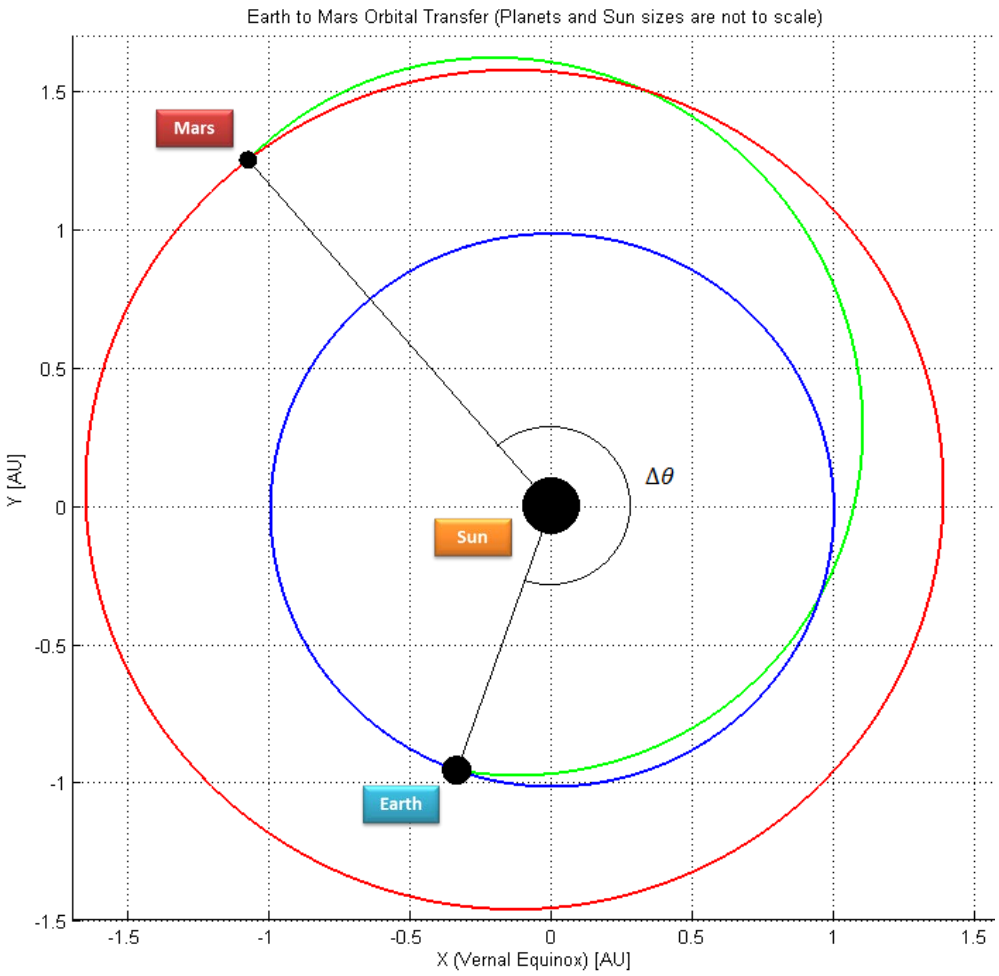

Figure 13 – Example of a Type II transfer with launch on June 1, 2020 and arrival on May 16, 2021.

ΔV vs. Departure Date vs. Arrival Date

Once $C3$ at departure and v_∞ at arrival have been calculated for all the possible combinations of dates of interest, as explained in Chapter 3, it is possible to calculate Δv_1 and Δv_2, the Earth departure and Mars arrival Δv's respectively, using Eq. (39) and Eq. (42). Then, using Eq. (47), Δv_{tot} can be found for all the range of dates. Figure 14 shows a contour plot of Δv_{tot} for the same ranges of dates used for the porkchop plot of Figure 11. In this case, an initial

Earth-centered circular parking orbit with an altitude of 300 km and a final Mars-centered circular parking orbit with an altitude of 200 km were considered.

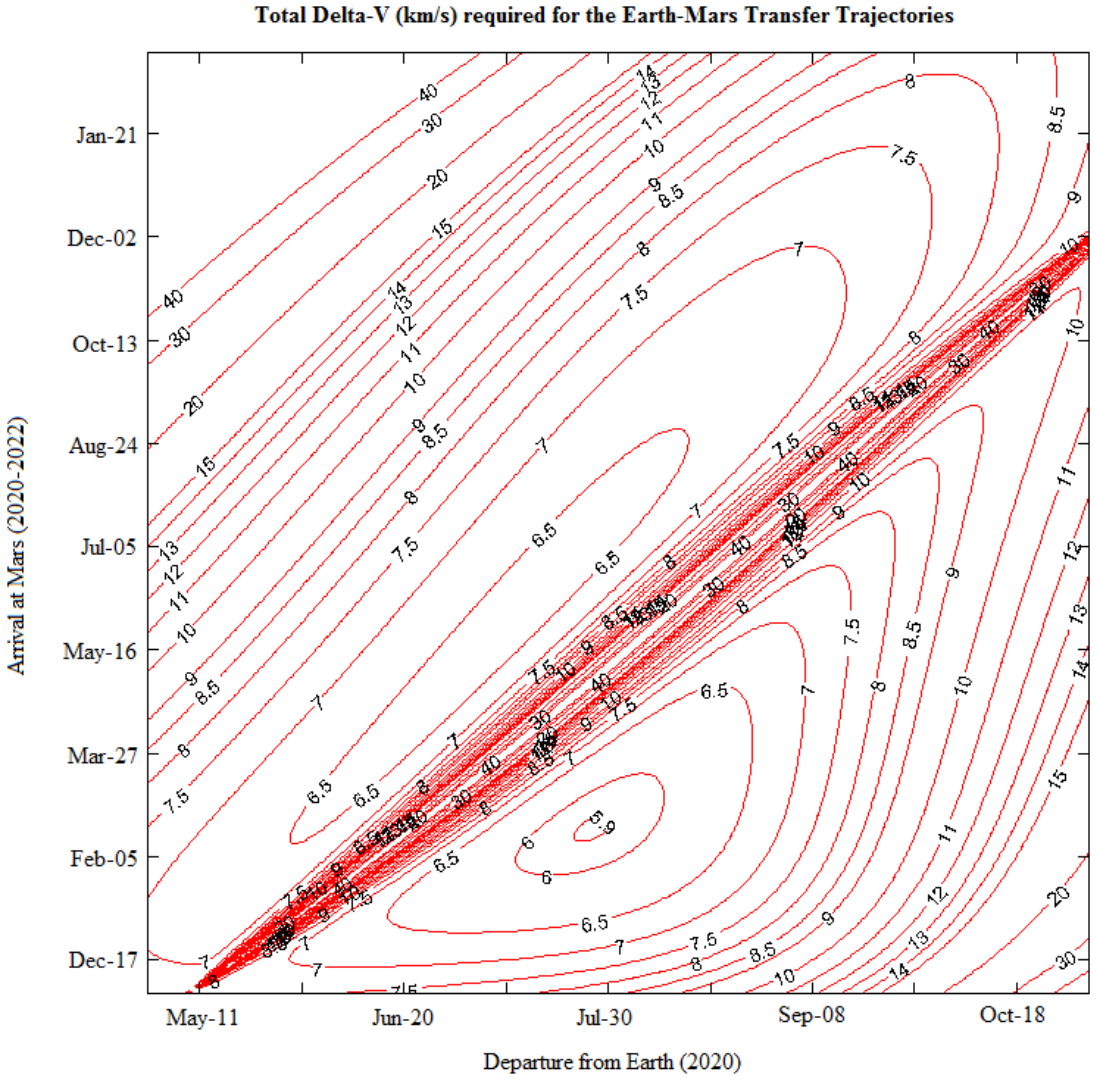

Figure 14 – ΔV_{tot} for the 2020-2022 Earth-Mars transfer trajectories.

From the Δv_{tot} plot the transfer dates that require the least Δv and hence the least amount of propellant can be found. For example, for the 2020-2022 timeframe Figure 14, Table 4 summarizes the key results. Notice that this particular value of Δv_{tot} is a minimum for the type I transfer orbit presented in Figure 14.

Table 4 – Key results of the Earth-Mars trajectory that minimizes ΔV_{tot} in the 2020-2022 timeframe.

Earth-Mars Trajectories for the 2020-2022 timeframe – Minimum ΔV	
Parameter	**Value**
Δv_{tot}	5.8921 km/s
C3 at Launch	14.045 km^2/s^2
v_∞ at Arrival	2.5748 km/s
Departure Date	July 27, 2020
Arrival Date	February 19, 2021
Time of Flight	207 days

Additionally, it is worth noting that the combination of dates at which the minimum Δv_{tot} happens is usually not where the minimum C3 at launch and minimum v_∞ at arrival occur, although lower values of C3 and v_∞ tend to give lower values of Δv_{tot}.

Propellant Mass

Knowing the required Δv_{tot} for the interplanetary transfer, propellant mass as a percentage of the total spacecraft mass can be easily obtained using Eq. (50). Additionally, as mentioned in Chapter 3, the I_{sp} of the propulsion system used for the main mission transfer must also be known (or estimated). Using an I_{sp} of 350 seconds and considering the 2020-2022 timeframe results into Figure 15. Notice that, as expected, the minimum propellant mass required occurs where the minimum Δv_{tot} occurs.

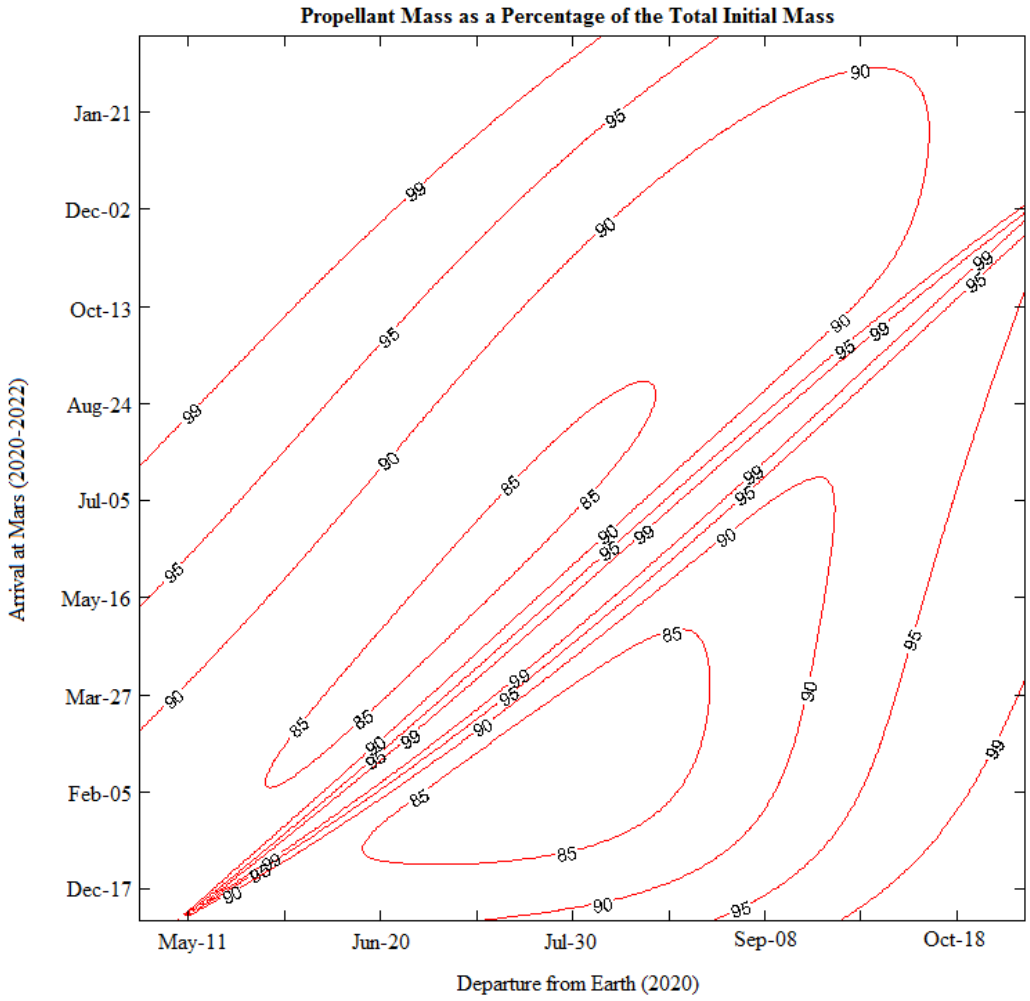

Figure 15 – Propellant mass as a percentage of total initial mass for the 2020-2022 timeframe.

Chapter 5

Targeting the Moons of Mars

Once the solution to Lambert's problem has been determined, the resulting arrival $\vec{v}_\infty$ can be used to determine the arrival trajectory within the sphere of influence of Mars. In order to accomplish this, all the known vector quantities must be converted to the same Mars inertial reference frame. In fact, since the orbital inclination of the arrival trajectory with respect to Mars' equatorial plane must be determined, the use of the Mars Mean Equatorial (MME) reference frame derived in the next section is most suitable. The process of converting the solution to Lambert's problem from J2000 Ecliptic to MME is done via the use of the Earth Mean Equatorial reference frame (EME).

Earth Mean Equatorial Inertial Reference Frame

The Earth Mean Equatorial reference frame, or EME, is a right-handed inertial reference frame defined as follows (see Figure 16):

$+\hat{Z}_{EME}$ is normal to the Earth mean equator of epoch J2000

$+\hat{X}_{EME}$ is parallel to the vernal equinox of the Earth mean orbit at J2000

$+\hat{Y}_{EME}$ completes the right-handed system such that $+\hat{Y}_{EME} = +\hat{Z}_{EME} \times +\hat{X}_{EME}$

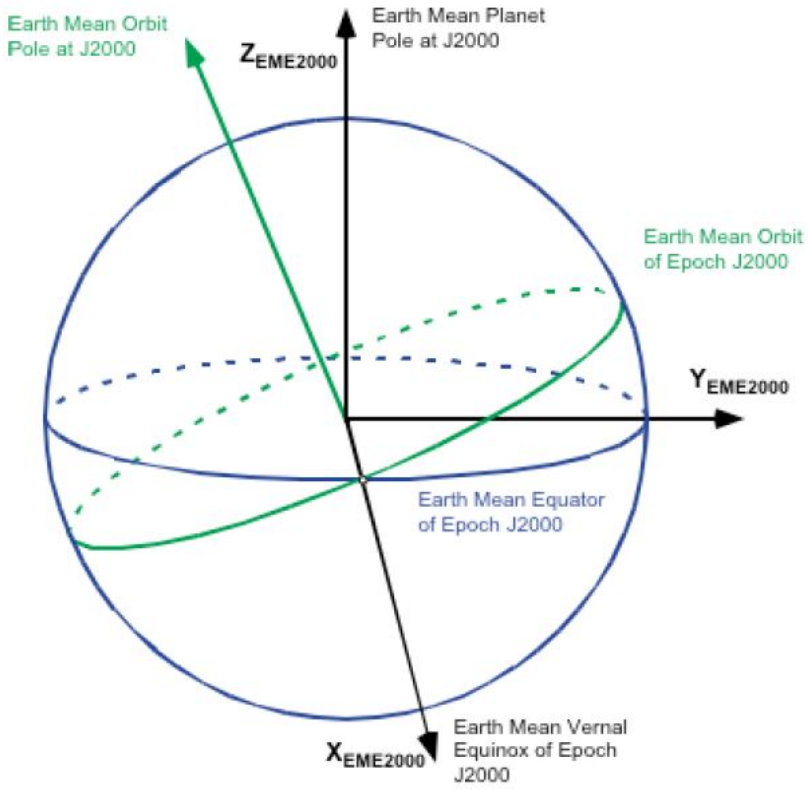

Figure 16 – Earth Mean Equatorial coordinate frame. Here, the subscript '2000' indicates the J2000 epoch. Source: Burkhart, p. 5.[1]

In order to convert from the J2000 Ecliptic to EME, one simple rotation is necessary. In fact, because the ecliptic plane is defined to be the orbital plane of Earth about the Sun, the only change in orientation of the EME with respect to the J2000 Ecliptic frame is the obliquity of the Earth. For the applications considered in this thesis, the obliquity of the Earth is given by

$$\epsilon_{Earth} = 23.43928° \tag{51}$$

where the time dependence of ϵ_{Earth} has been ignored. Knowing the value of Earth's obliquity permits to compute the direction cosine matrix that transforms from the Ecliptic to the EME references frames as follows:

$$C^{EclE} = \begin{bmatrix} 1 & 0 & 0 \\ 0 & \cos\epsilon_{Earth} & \sin\epsilon_{Earth} \\ 0 & -\sin\epsilon_{Earth} & \cos\epsilon_{Earth} \end{bmatrix} = \begin{bmatrix} 1 & 0 & 0 \\ 0 & 0.917482 & 0.397777 \\ 0 & -0.397777 & 0.917482 \end{bmatrix} \tag{52}$$

where the superscript EclE stand for "Ecliptic to EME."

The next section illustrates how to relate the EME and MME reference frames.

Mars Mean Equatorial Inertial Reference Frame

For convenience, it is useful to derive an inertial reference frame based on Mars' equator and analyze the arrival trajectories in such frame of reference. Such coordinate frame is given in terms of Earth Mean Equator, or EME. The EME reference frame is a right-handed coordinate system defined as follows:

$+\hat{Z}_{EME}$ is normal to the Earth mean equator of epoch J2000

$+\hat{X}_{EME}$ is parallel to the vernal equinox of the Earth mean orbit at J2000

$+\hat{Y}_{EME}$ completes the right-handed system such that $+\hat{Y}_{EME} = +\hat{Z}_{EME} \times +\hat{X}_{EME}$

The direction of the Martian North pole with respect to the EME reference frame is given in degrees in terms of right ascension, RA, and declination, DEC, as follows[1]:

$$RA = 317.68143° - 0.1061T \tag{53}$$

$$DEC = 52.8865° - 0.0609T \tag{54}$$

where T is the time in Julian centuries of 36525 days past the reference epoch of J2000. The time dependence of RA and DEC is very small if compared to the years past from the year 2000 and considering the times of flight of the various trajectories in analysis. Therefore, the terms depending on T are negligible and thus ignored.

Converting the given values of RA and DEC given by Eq. (53) and (54) into Cartesian coordinates and ignoring the time dependence results in the direction of the Mars pole vector:

$$\hat{Z}_{MME} = Mars\ pole = (0.446159, -0.406238, 0.797442) \tag{55}$$

For practical reasons the vector was normalized to be a unit vector. The subscript MME stands for Mars Mean Equator. In order to define a coordinate frame, at least two perpendicular unit vectors must be specified. Therefore, the Mars vernal equinox direction must be determined. This

can be done by finding the direction of the mean Mars orbit angular momentum vector. At J2000 the position and velocity directions (i.e. unit vectors) of Mars can be found in the Sun-centered EME reference frame by applying Standish's method as:

$$\hat{r}_{Mars}^{EME} = (0.999647, 0.001007, -0.026567) \tag{56}$$

$$\hat{v}_{Mars}^{EME} = (0.044163, 0.908515, 0.415513) \tag{57}$$

Using the definition of angular momentum and the quantities given in Eq. (54) and (55) it is possible to define the position of the Martian orbit pole:

$$orbit\ pole = \hat{r}_{Mars}^{EME} \times \hat{v}_{Mars}^{EME} = (0.024569, -0.416780, 0.908675) \tag{58}$$

Note that the orbit pole vector was normalized.

The Vernal Equinox of Mars is defined as the normalized cross product between the Mars geographic North pole given by Eq. (55) and the orbit pole given by Eq. (58):

$$\hat{X}_{MME} = vernal\ equinox = mars\ pole \times orbit\ pole =$$
$$(-0.086410, -0.906433, -0.413415) \tag{59}$$

In order to complete the reference frame, the unit vector $\hat{Y}_{MME}$ can be obtained by computing the cross product between $\hat{Z}_{MME}$ and $\hat{X}_{MME}$ as follows:

$$\hat{Y}_{MME} = \hat{Z}_{MME} \times \hat{X}_{MME} = (0.890773, 0.115542, -0.4395160) \tag{60}$$

Figure 17 shows the orientation of $\hat{X}_{MME}$, $\hat{Y}_{MME}$ and $\hat{Z}_{MME}$ with respect to Mars. Note that this reference frame does not rotate with Mars but it is fixed in the inertial space relative to the Solar System.

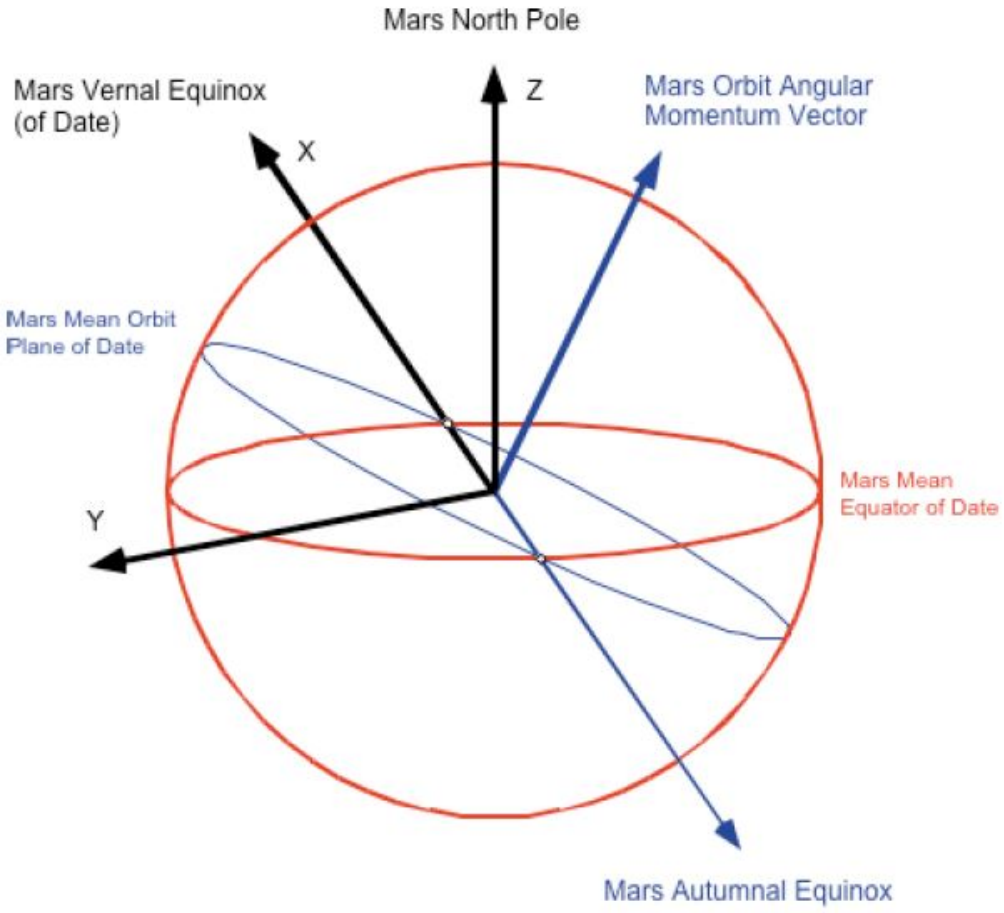

Figure 17 – Mars Mean Equatorial reference frame. Source: Burkhart, p. 7.[1]

Therefore, it is now possible to define the Mars Mean Equator inertial reference frame in terms of the Earth Mean Equator inertial reference frame. From this relationship, the direction cosine matrix to transform any vector from EME to MME can be constructed as follows:

$$C^{EM} = \begin{bmatrix} \hat{X}_{MME} \\ \hat{Y}_{MME} \\ \hat{Z}_{MME} \end{bmatrix} \tag{61}$$

Substituting for the values of $\hat{X}_{MME}$, $\hat{Y}_{MME}$ and $\hat{Z}_{MME}$ yields to:

$$C^{EM} = \begin{bmatrix} -0.086410 & -0.906433 & -0.413415 \\ 0.890773 & 0.115542 & -0.439516 \\ 0.446159 & -0.406238 & 0.797442 \end{bmatrix} \tag{62}$$

Hence, using Eq. (52) and (62), one can convert any vectors (and in particular $\vec{v}_\infty$ obtained from solving Lambert's problem) from the J2000 Ecliptic frame to the MME frame as follows:

$$\vec{v}_\infty^{MME} = C^{EM}C^{EclE}\vec{v}_\infty^{Ecl} = \begin{bmatrix} -0.086410 & -0.667189 & -0.739859 \\ 0.890773 & 0.280837 & -0.357288 \\ 0.446159 & -0.689920 & 0.570047 \end{bmatrix} \vec{v}_\infty^{Ecl} \tag{63}$$

B-Plane

When sending a spacecraft to a celestial body in the Solar System, one reference frame often used upon arrival is the B-plane (Body Plane) frame. It is useful to analyze B-plane parameters especially when considering targeting specific orbits within the sphere of influence of the arrival planet.

The B-Plane is defined as a plane which is normal to the $\vec{v}_\infty$ and that contains the target body's center of mass. Here, "infinity" is defined to be far enough away from the vertex of the hyperbola, such that the trajectory essentially lies on the asymptote of the arrival hyperbolic orbit. For practical reasons, "far enough away" is the boundary of the sphere of influence such that the magnitude of the position vector of the spacecraft is r_{SOI} as given by Eq. (44). $\hat{B}$ is a unit vector that points from the origin (arrival body's center of mass) to that point where the asymptote (or $\vec{v}_\infty$) intersects the B-plane. $\hat{S}$ is a unit vector that is normal to the B-plane and it is collinear to $\vec{v}_\infty$. $\hat{T}$ is a unit vector normal to the $\hat{S}$ and it typically lies on the body's equatorial plane. $\hat{R}$ is given by $\hat{R} = \hat{S} \times \hat{T}$ and it points in the direction of the south pole of the body if $\hat{T}$ and $\hat{S}$ lie on the equatorial plane.

Figure 18 shows the geometry of the B-plane with its associated parameters. Note that for Earth-Mars trajectories, the orientation and magnitude of $\vec{v}_\infty$ are given by the solution to Lambert's problem which depends on the departure and arrival dates. Because of this fact, the B-

plane is not uniquely defined between Earth and Mars and its orientation is therefore time dependent. A complete derivation of the B-plane reference frame can be found in Jah.[7]

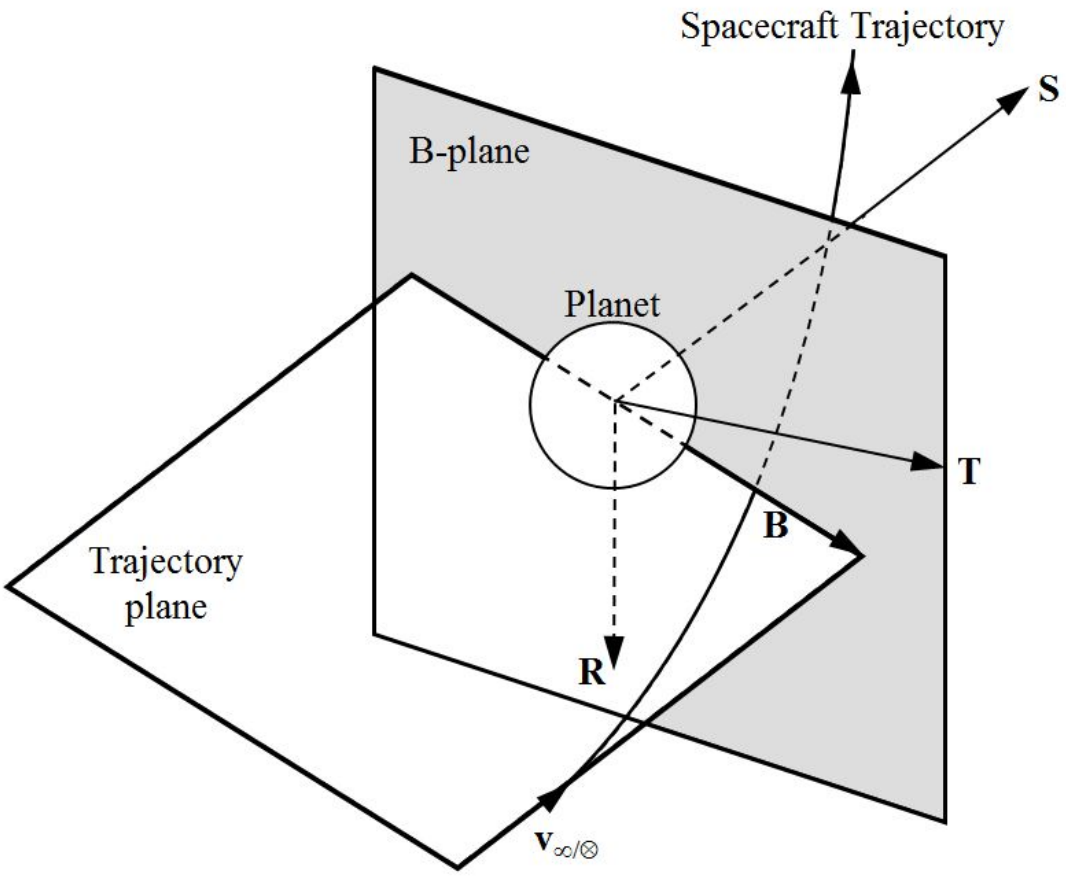

Figure 18 – Geometry of the B-plane and its associated parameters.

Determining the Orientation of the Arrival Trajectory

Since solving Lambert's problem for interplanetary trajectories made use of the patched conics approximation (i.e. the sphere of influence of Mars is negligible), virtually infinite Mars arrival trajectories exist for a given $\vec{v}_\infty$. Therefore, it is necessary to define two orbital parameters for the arrival trajectories to constrain the analysis to yield a unique solution for each Earth departure and Mars arrival dates. A logical choice would be to fix the periapse location to be a

value close to one of the semi-major axis of the moons of Mars. For example, if one wishes to insert a spacecraft in an orbit close to that of Phobos (SMA = 9378 km from Table 1), a periapse of about 9500 km should be chosen. Additionally, assuming that both Phobos and Deimos have equatorial circular orbits with respect to Mars implies that the argument of periapse can arbitrarily be set to 0 degrees, i.e. $\omega = 0°$ using standard notation. From the definition of ω:

$$\omega = \pm\cos^{-1}\left(\frac{\vec{e}\cdot\hat{n}}{e}\right) \tag{64}$$

one can see that $\omega = 0°$ implies that periapsis occurs when the orbital plane intersects the node vector, $\hat{n}$.

As previously mentioned, the orbital inclination of the arrival trajectory with respect to Mars is a key design parameter. In fact, performing pure inclination changes are rather "propellant expensive" since the ΔV required to accomplish such task is given by:

$$\Delta v_i = 2v\sin\frac{\Delta i}{2} \tag{65}$$

where v is the velocity of the spacecraft where Δv_i is performed, i.e. either where the orbital plane intersect the ascending node or descending node for pure inclination changes.

In order to avoid having to perform relatively large Δv_i, trajectories that lead to a small value of inclination should be chosen.

Inclination of the Arrival Trajectory

As previously stated, one of the main design parameters in targeting the moons of Mars is the orbital inclination of the arrival orbit. Determining the orbital inclination can then be done by relating $\vec{v}_\infty$ in the B-plane frame:

$$\frac{\vec{v}_\infty^{B-Plane}}{|\vec{v}_\infty^{B-Plane}|} = \hat{S} = \begin{bmatrix}0\\1\\0\end{bmatrix} \tag{66}$$

Since in B-Plane coordinates $\vec{v}_\infty$ has only one component and since $\hat{S}$ lies on Mars' equatorial plane, using the standard 3-1-3 rotation that transforms from a planet-centered inertial frame to perifocal frame yields to:

$$\frac{1}{|\vec{v}_\infty|}\begin{bmatrix} v_{\infty,X}^{MME} \\ v_{\infty,Y}^{MME} \\ v_{\infty,Z}^{MME} \end{bmatrix} = \begin{bmatrix} \sin\Omega\cos\omega + \cos\Omega\sin\omega\cos i \\ -\sin\Omega\sin\omega + \cos\Omega\cos\omega\cos i \\ -\cos\Omega\sin i \end{bmatrix} \tag{67}$$

Using the fact that $\omega = 0°$ and dividing the z-component by the y-component results in the following:

$$i = -\tan^{-1}\left(\frac{v_{\infty,Z}^{MME}}{v_{\infty,Y}^{MME}}\right) \tag{68}$$

In order to resolve the quadrant ambiguity, the MATLAB function atan2 can be used in place of the traditional arctangent function. Thus, Eq. (68) becomes:

$$i = -\text{atan2}(v_{\infty,Z}^{MME}, v_{\infty,Y}^{MME}) \tag{69}$$

Since orbital inclination is usually defined in the range $[0°, 180°]$, Eq. (69) can be further modified to map the values obtained from Eq. (69), which are always within the range $[-90°, 90°]$, to $[0°, 180°]$. Only prograde orbits were considered for the arrival trajectories.

Note that this result for inclination implies that, as expected, small inclinations are given by small values of $v_{\infty,Z}^{MME}$. This corresponds to having small values of out-of-Mars equatorial plane component of $\vec{v}_\infty^{MME}$.

Calculating Total ΔV at Periapsis

In order to calculate the total ΔV required to be captured upon arrival and change the orbital inclination at the same time, a ΔV maneuver at periapsis was considered as shown in Figure 19. In fact, since the argument of periapsis, ω was set to zero, the ascending/descending

node occurs at periapsis. In Figure 19, $\vec{v}_{sc,p-arr}$ is the velocity the spacecraft has at periapsis on the hyperbolic orbit, $\vec{v}_{sc,c-final}$ represents the final desired velocity of the circular orbit about Mars, and $\Delta\vec{v}_{i,tot}$ is the vector difference of $\vec{v}_{sc,p-arr}$ and $\vec{v}_{sc,c-final}$, i.e.

$$\Delta\vec{v}_{i,tot} = \vec{v}_{sc,p-arr} - \vec{v}_{sc,c-final} \tag{70}$$

Using the law of cosines, it is possible to calculate the magnitude of $\Delta\vec{v}_{i,tot}$ as follows:

$$|\Delta\vec{v}_{i,tot}| = \sqrt{\left(v_{sc,p-arr}\right)^2 + \left(v_{sc,c-final}\right)^2 - 2v_{sc,p-arr}v_{sc,c-final}\cos i} \tag{71}$$

Here, since the final desired inclination is zero, $\Delta i = i$.

As stated in Chapter 1, one could take advantage of "closing" the arrival hyperbolic orbit just barely and make an inclination change at apoapsis, but a small underperformance in the propulsion system could cause the spacecraft to still be on an escape trajectory compromising the success of the mission. Additionally, since small values of inclination are considered, the out-of-orbital-plane component is also.

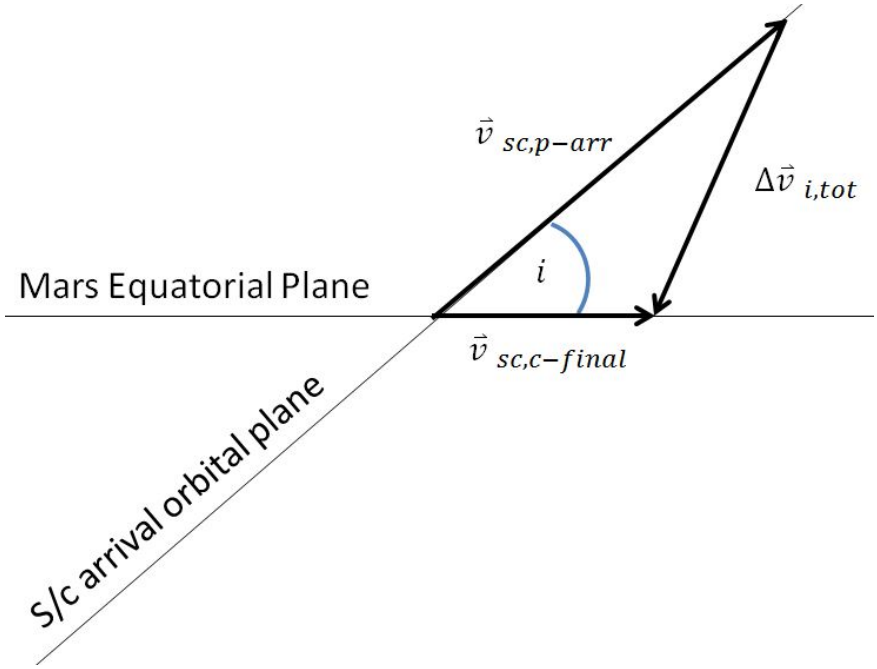

Figure 19 – Geometry of the arrival trajectory and the required ΔV to be captured in a Mars equatorial orbit.

Right Ascension of the Ascending Node of the Arrival Trajectory

In order to uniquely determine the orientation of the arrival trajectory in the MME reference frame, the value of Ω must be known. Note that Ω defines the location of the ascending node of the spacecraft orbit with respect to $\hat{X}_{MME}$. Using Eq. (67) and knowing the values of i (see previous section) and that $\omega = 0$, it is possible to solve for the value of Ω and obtain the following relations:

$$\sin\Omega = \frac{v_{\infty,X}^{MME}}{1+v_{\infty,Y}^{MME}} \tag{72}$$

$$\cos\Omega = \frac{v_{\infty,Y}^{MME}}{\cos i} \tag{73}$$

Thus, diving Eq. (72) by Eq. (73) yields to:

$$\tan\Omega = \frac{\cos i v_{\infty,X}^{MME}}{v_{\infty,Y}^{MME}\left(1+v_{\infty,Y}^{MME}\right)} \tag{74}$$

Similarly to what was done for determining inclination, the function atan2 can be used and the resulting values can be mapped from $[-180°, 180°]$ to $[0°, 360°]$ as follows:

$$\Omega = \begin{cases} \text{atan2}\left[\cos i\, v_{\infty,X}^{MME}, v_{\infty,Y}^{MME}\left(1+v_{\infty,Y}^{MME}\right)\right] & if\ \text{atan2}[\,] \geq 0 \\ \text{atan2}\left[\cos i\, v_{\infty,X}^{MME}, v_{\infty,Y}^{MME}\left(1+v_{\infty,Y}^{MME}\right)\right] + 360° & if\ \text{atan2}[\,] < 0 \end{cases} \tag{75}$$

Eccentricity of the Arrival Trajectories and Turn Angle

Other important parameters of the arrival trajectories at Mars are the eccentricity and the turn angle. The latter is particularly of interest to know the orientation of the B-plane with respect to the MME reference frame. Figure 20 shows the geometry of the arrival trajectory with an emphasis on turn angle.

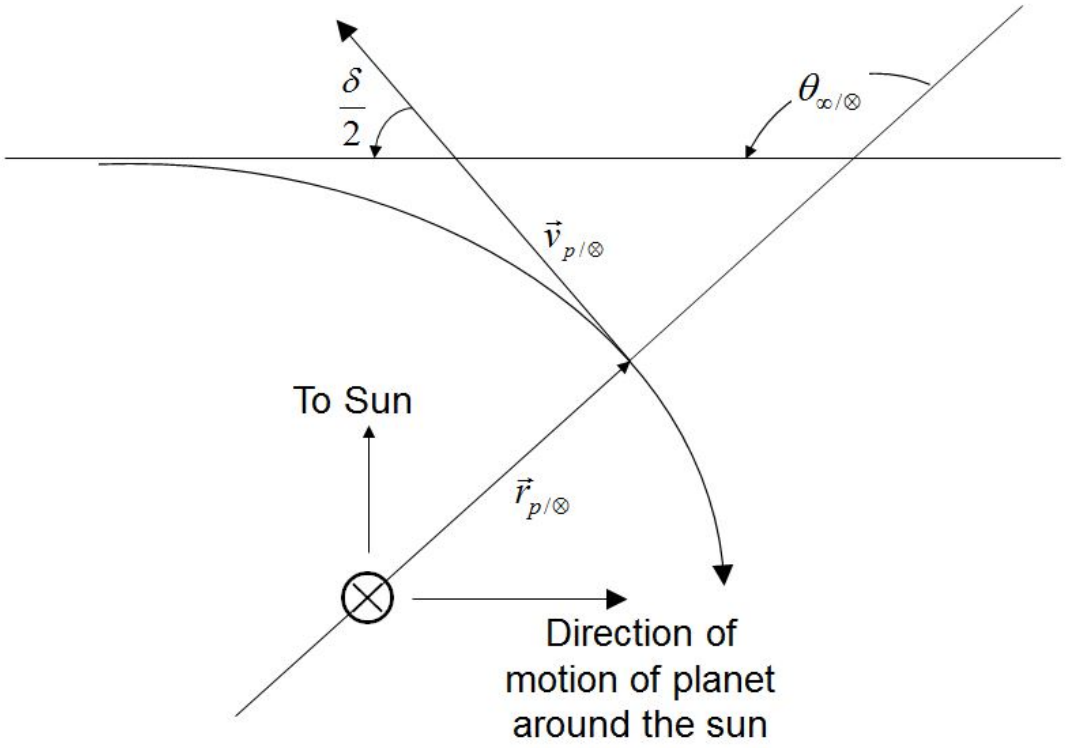

Figure 20 – Geometry of the arrival hyperbolic trajectory highlighting the turn angle, δ.

Eccentricity and turn angle can be calculated using the following expressions:

$$e = 1 + \frac{r_{p/Mars}\left(v_{\infty/Mars}\right)^2}{\mu_{Mars}} \tag{76}$$

$$\delta = 2\sin^{-1}\left(\frac{1}{e}\right) \tag{77}$$

More details regarding the rendezvous with Phobos or Deimos are discussed in Chapter 6.

Chapter 6

Finding the Optimal Launch-Arrival Window

In this chapter, the algorithms and analysis presented previously have been combined to obtain various results to determine the optimal launch and arrival date to target the moons of Mars. Figures 21 – 24 refer to the same departure/arrival combination used in Chapter 4. Here, an altitude of 300 km for the Earth-centered circular parking orbit was considered while the final Mars-periapsis altitude of the arrival trajectory was set to a value of 6100 km which is slightly higher than the altitude at which Phobos orbits Mars. Refer to Figure 11 for the porkchop plot of this 2020-2022 Earth-Mars launch/arrival window. Note that the arrival inclination has been mapped to $[-90°, 90°]$ for ease of visualization. Positive values close to zero are preferable while negative values denote retrograde orbits which would make rendezvousing with Phobos extremely "Δv expensive".

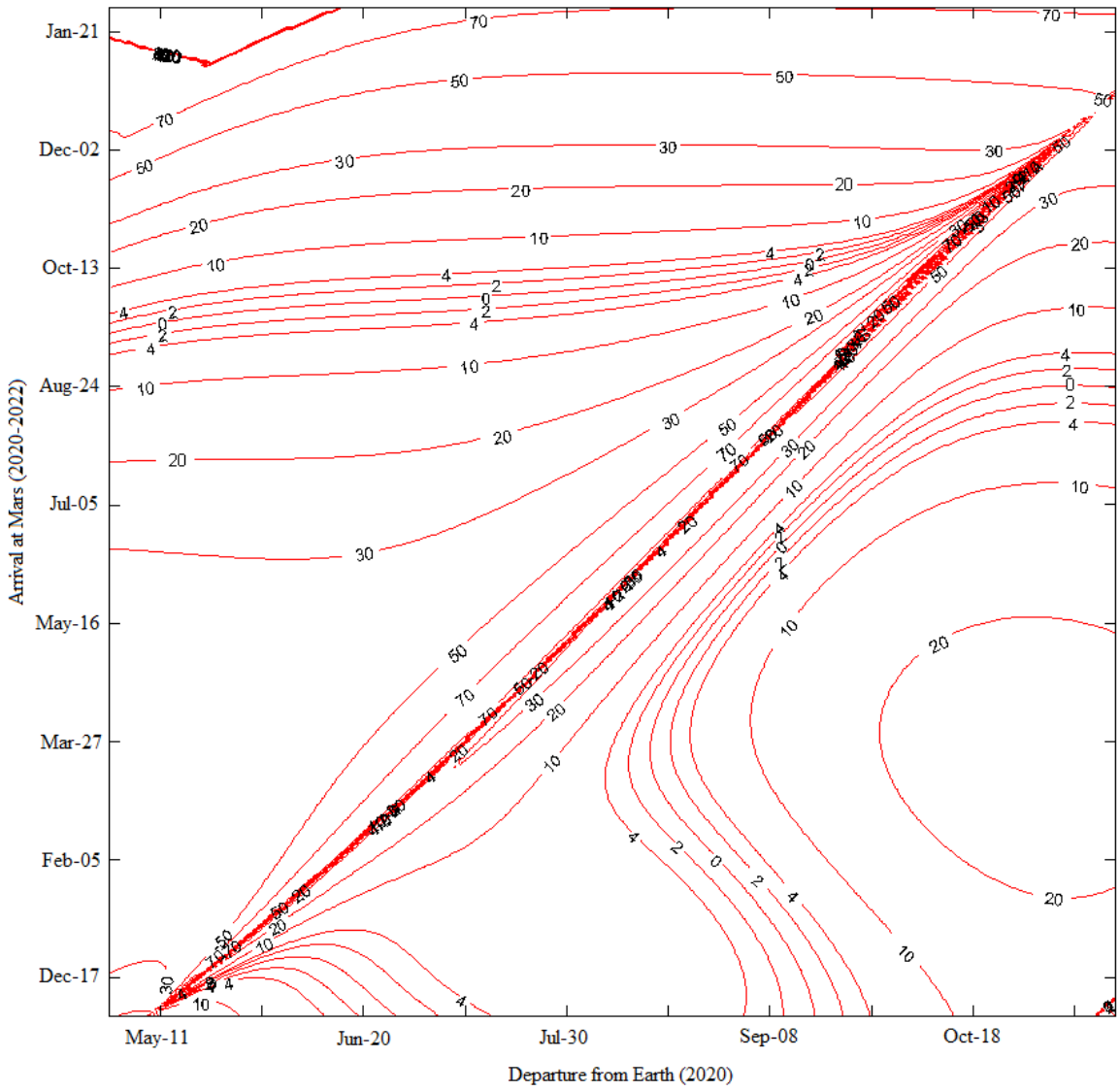

Figure 21 – Inclinations (in degrees) of the arrival trajectories with respect to the MME frame for the 2020-2022 timeframe.

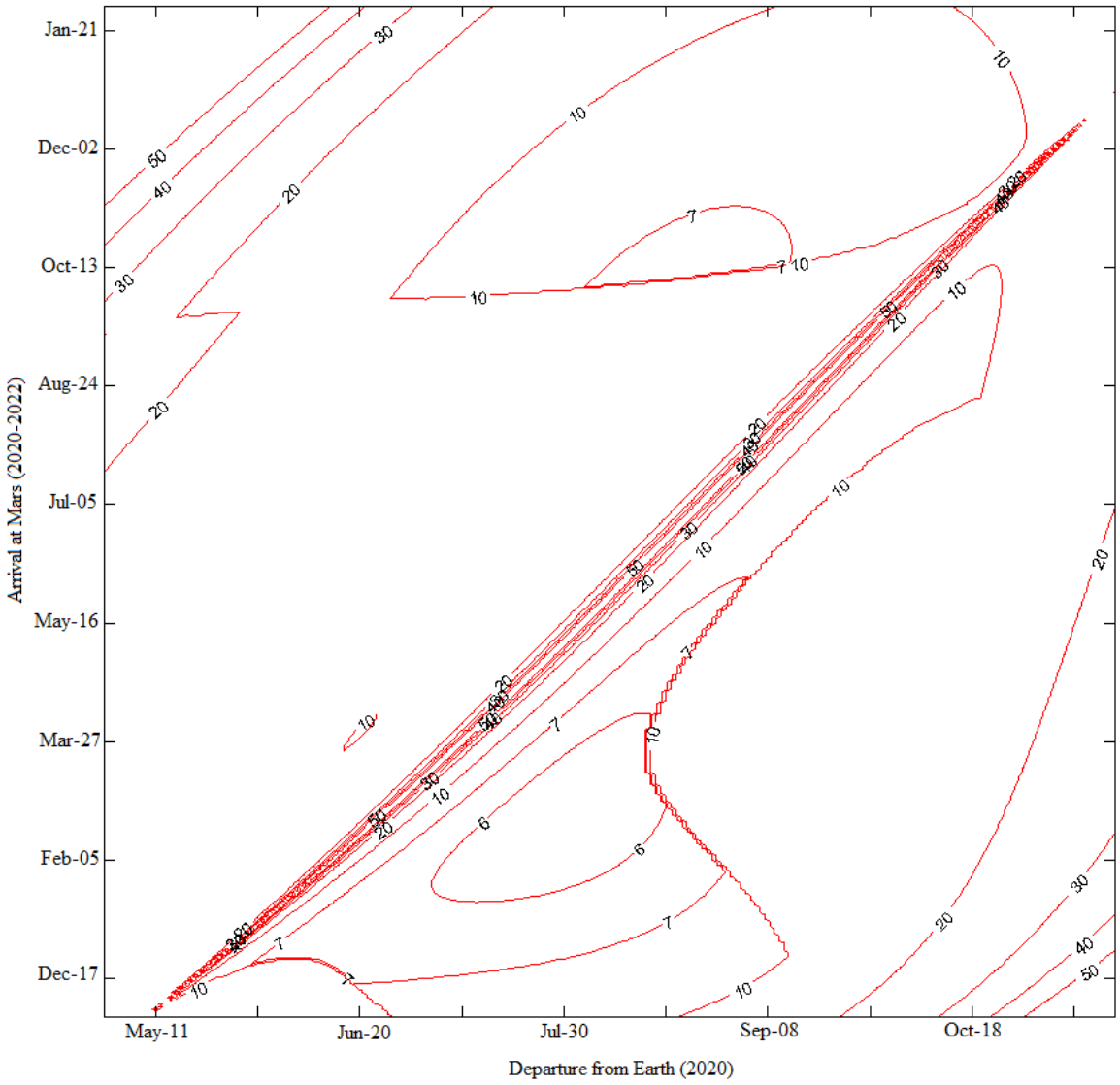

Figure 22 – Total Δv (in km/s) required for Earth-Phobos trajectories including inclination changes in the timeframe 2020-2022.

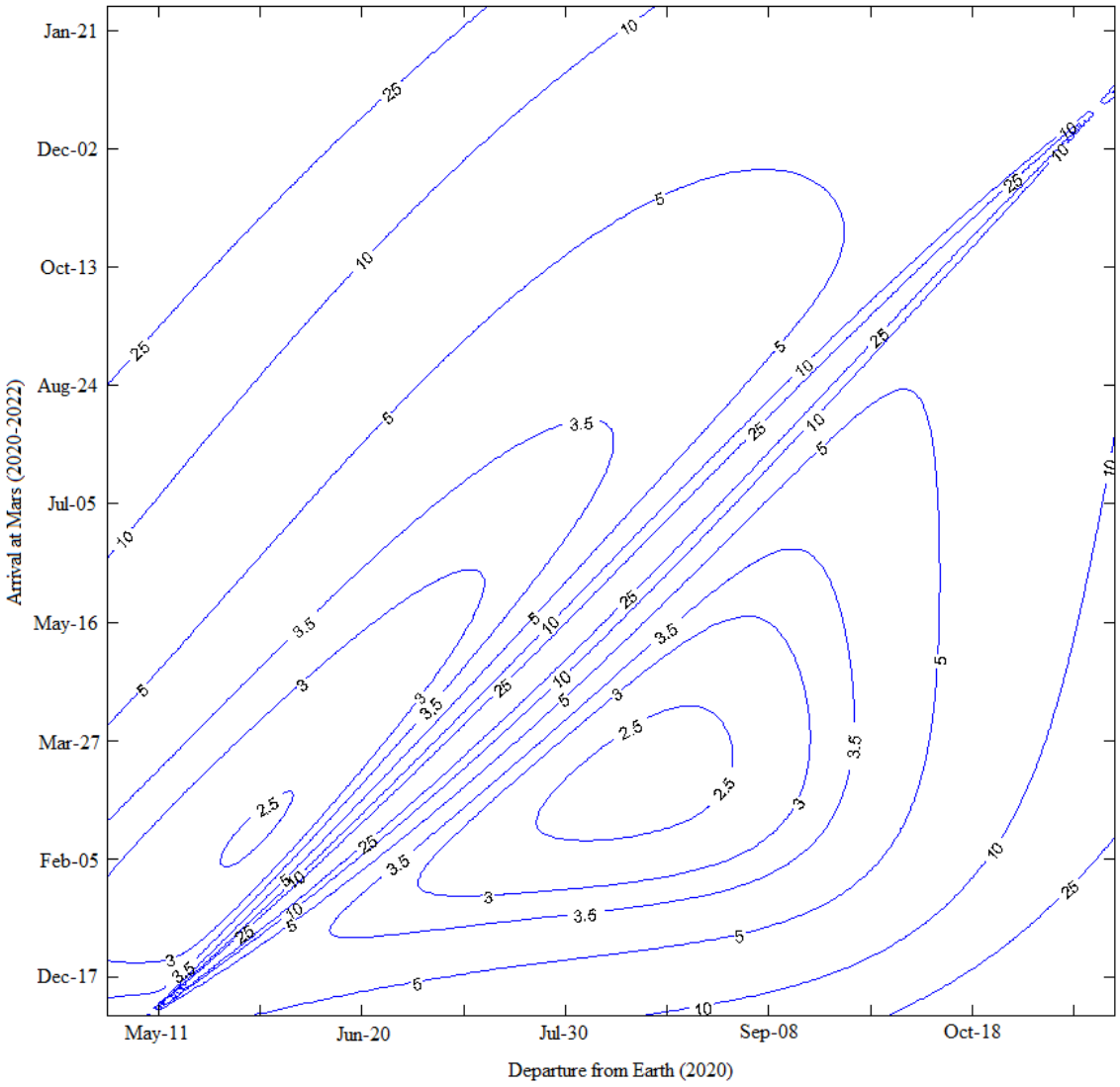

Figure 23 – Eccentricities of the arrival hyperbolic orbits.

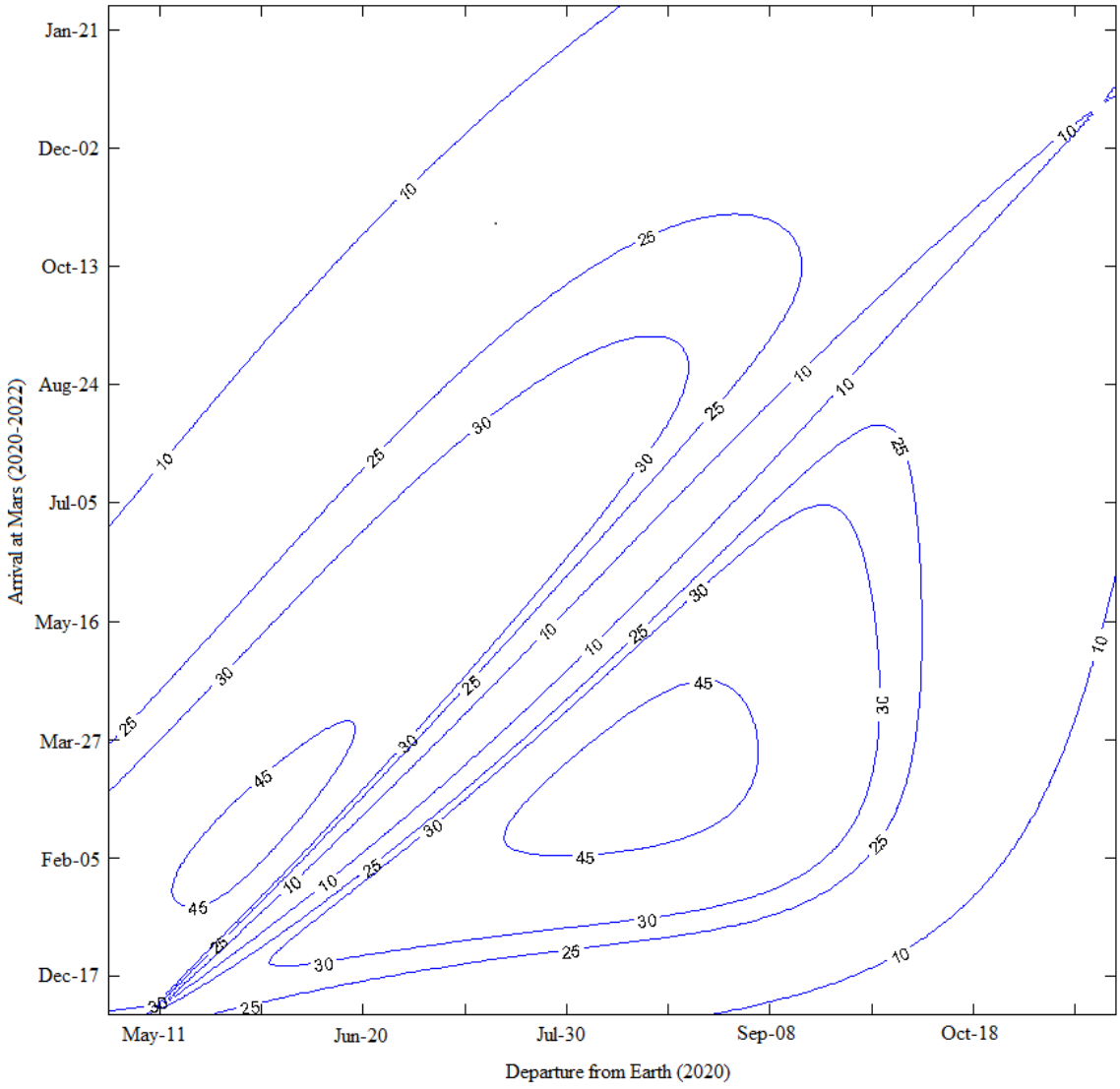

Figure 24 – Turn angles (in degrees) of the arrival trajectories.

Table 5 summarizes the important parameters of the Earth-Phobos trajectory for the minimum value of the total ΔV when an inclination change upon arrival is considered.

Table 5 – Key results of the Earth-Mars trajectory that minimizes ΔV_{tot} in the 2020-2022 timeframe considering an inclination change upon arrival.

Earth-Phobos Trajectories for the 2020-2022 timeframe – Minimum ΔV	
Parameter	**Value**
Δv_{tot}	5.6631 km/s
Arrival i (MME)	6.321°
C3 at Launch	14.881 km^2/s^2
v_∞ at Arrival	2.5227 km/s
Interplanetary a	1.3171 AU
Interplanetary e	0.231
Interplanetary i (J2000)	2.384°
Interplanetary ω (J2000)	350.61°
Interplanetary Ω (J2000)	−52.07°
Departure Date	July 31, 2020
Arrival Date	February 27, 2021
Time of Flight	211 days

Note that Δv_{tot} in Table 5 is smaller than that of Table 6 because the arrival altitude of the trajectories considered are considerably different (200 km vs. 6100 km). Moreover, the minimum Δv_{tot} does not occur when the inclination of the arrival orbit is minimized. For more details on the 2020-2022 timeframe arrival trajectories, see Appendix D. Figure 24 shows the interplanetary trajectory from Earth to Mars that satisfies the minimum Δv_{tot} conditions reported in Table 5. The blue, red and green curves represent the orbits of Earth and Mars, and the interplanetary trajectory from Earth to Mars respectively.

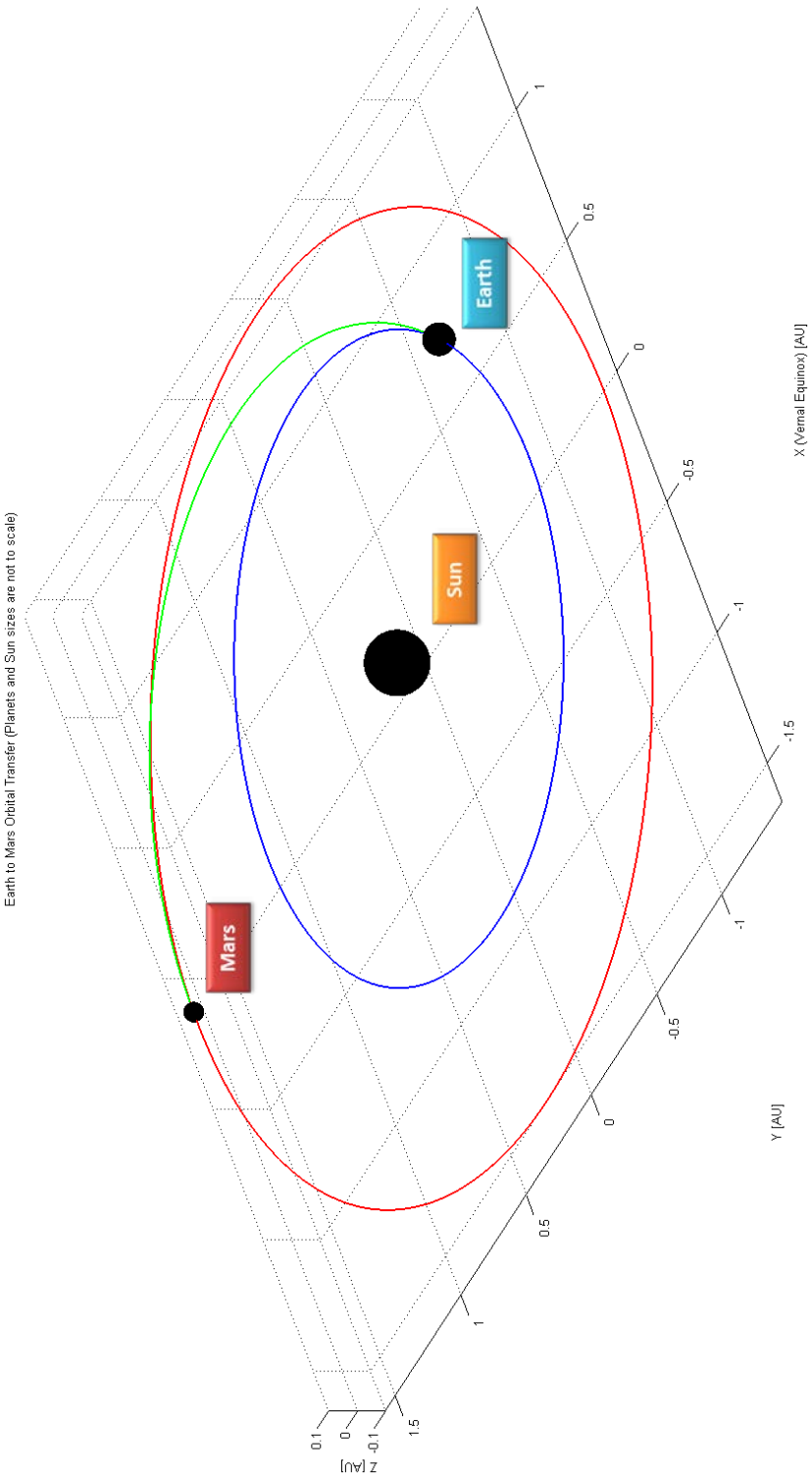

Figure 24 – Earth-Mars interplanetary trajectory for the minimum Δv_{tot} considering inclination changes upon arrival in the 2020-2022 timeframe.

Rendezvous with Phobos and Deimos

Once the spacecraft has been captured and is in a equatorial circular orbit about Mars with different altitude than the desired targeted moon, a Hohmann transfer can be used to minimize propellant use. Alternatively, Lambert's problem can be used to determine the 2-burn maneuver needed to arrive at Phobos or Deimos. Additionally, the use of the Clohessy-Wiltshire-Hill (CWH) equations can be considered if the spacecraft is in the vicinity of Phobos or Deimos.

Hopkins reports a mission to Phobos departing from Earth in April 17, 2033 and arriving on November 4, 2033 (with a TOF of 201 days). Maneuvers shown in Figure 3 and additional Δv's required to rendezvous with Phobos yield a total Δv of 2.017 km/s.[5] Furthermore, the bi-elliptic maneuver considered by Hopkins requires the spacecraft to wait 49 days after arrival before being able to rendezvous with Phobos. Two different cases were analyzed using both a Hohmann transfer (case 1) and a bi-elliptic transfer (case 2). For both cases the departure from Earth and arrival at Mars are July 31, 2020 and February 21, 2021 respectively. Table 5 summarizes the key parameters for such trajectory.

In the sphere of influence of Mars, case 1 results in a total Δv of 1.840 km/s including the necessary maneuvers to rendezvous with Phobos. Moreover, for the parameters taken into account, a Hohmann transfer from the arrival circular orbit to the orbit of Phobos would have a synodic period of approximately 17 days. This means that upon arrival, the maximum wait time before a rendezvous window opens is 17 days. On the other hand, the total Δv reported by Hopkins is slightly smaller than that of case 1 though, as previously mentioned in Chapter 1, a one-burn propulsive maneuver for Mars orbit insertion would be safer and faster.

Case 2 considers a similar maneuver to that presented by Hopkins with the same arrival periapsis and bi-elliptic apoapsis. Although the time from orbit insertion to being able to

rendezvous with Phobos is 49 days, case 2 results in a total Δv about Mars of 1.575 km/s. This makes case 2 the lowest total mission Δv of the cases that were considered.

Case 1 is shown in Figure 26 and Figure 27 and case 2 is shown in Figure 28 and Figure 29. Note that the size of Phobos (both cases) and the orbit of the spacecraft after being captured (case 1) are not to scale. They were made larger for visualization purposes. Additionally, the comparison between Hopkins' results and case 1 and case 2 are summarized in Table 6.

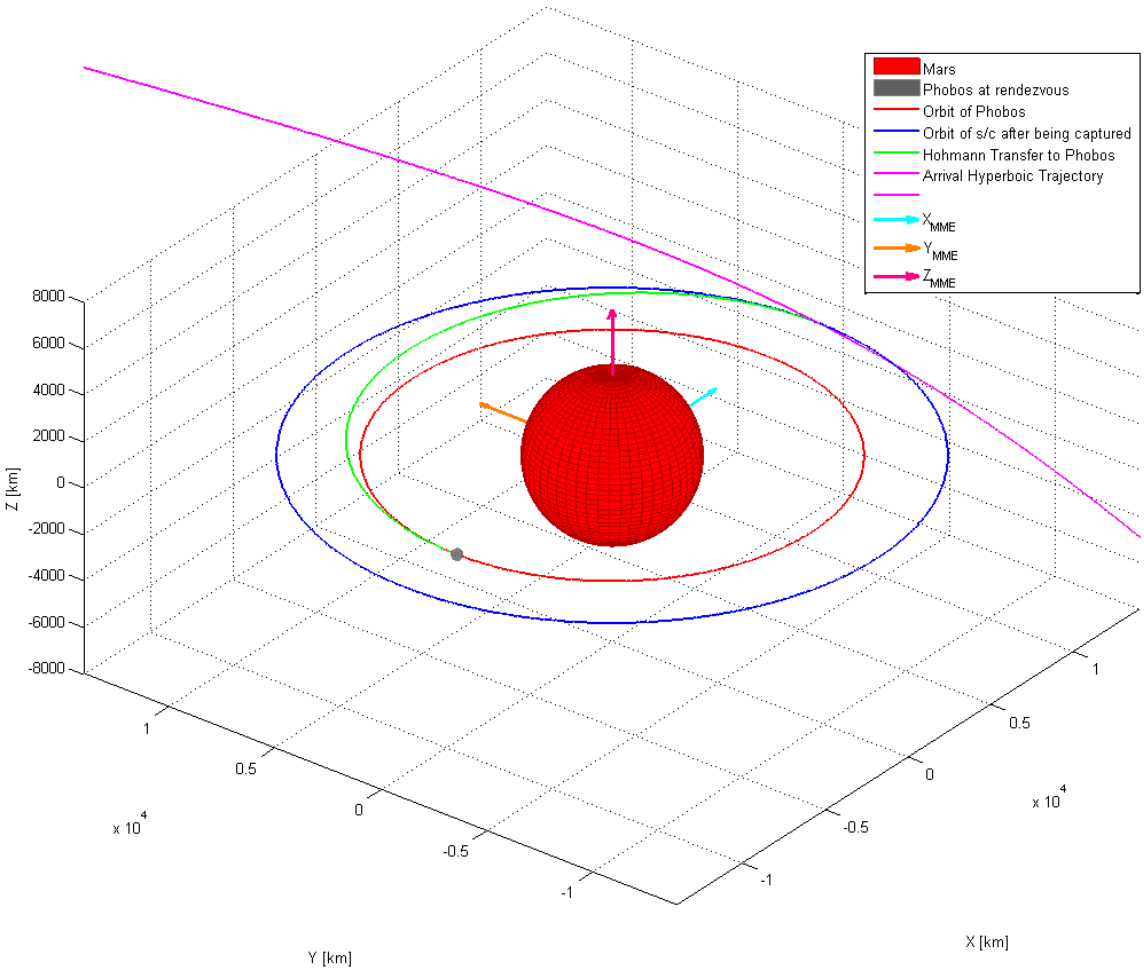

Figure 26 – Arrival scenario for the minimum ΔV case (2020-2022 timeframe) using a Hohmann transfer to rendezvous with Phobos.

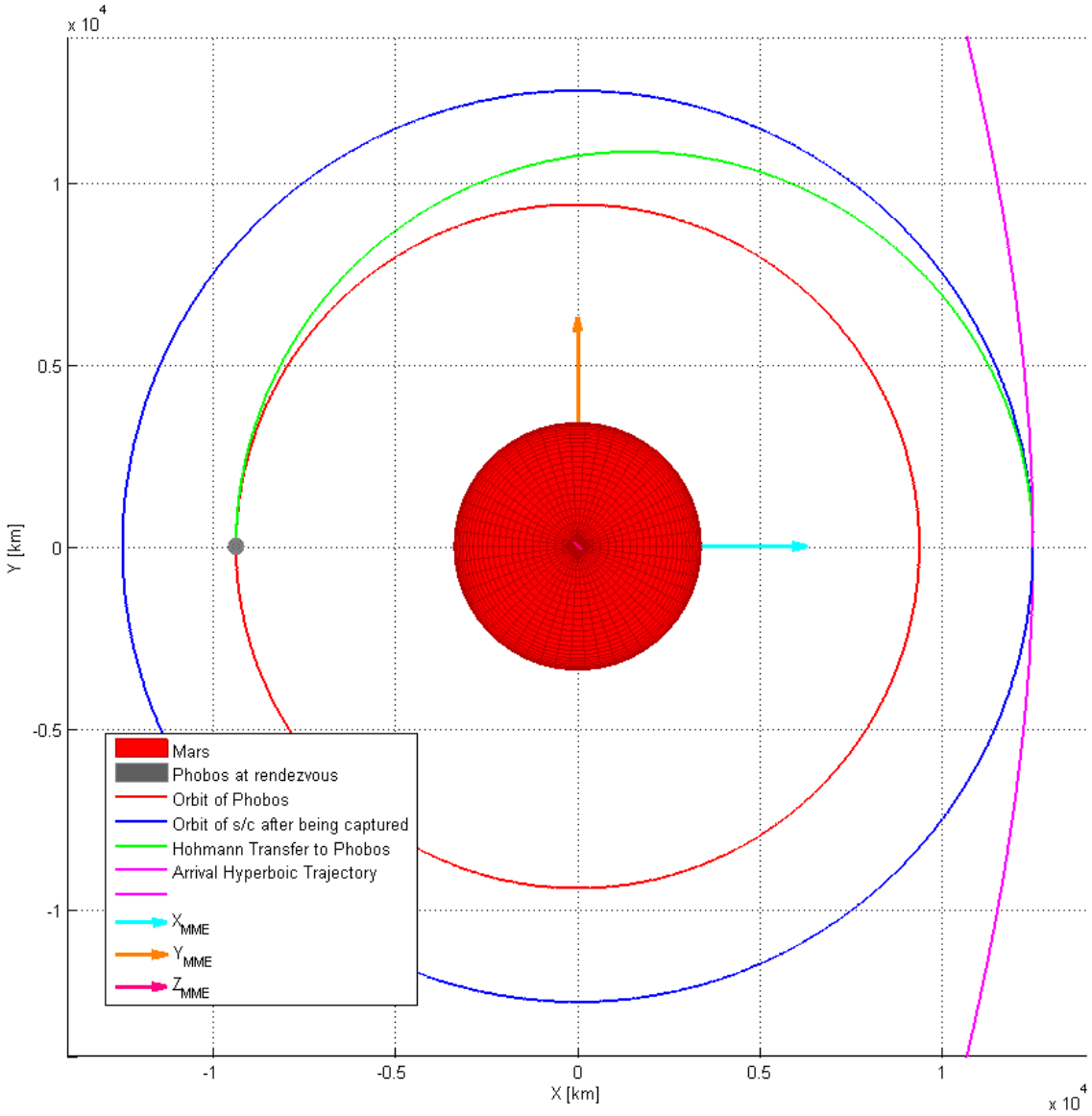

Figure 27 – Arrival scenario (top view) for the minimum ΔV case (2020-2022 timeframe) using a Hohmann transfer to rendezvous with Phobos.

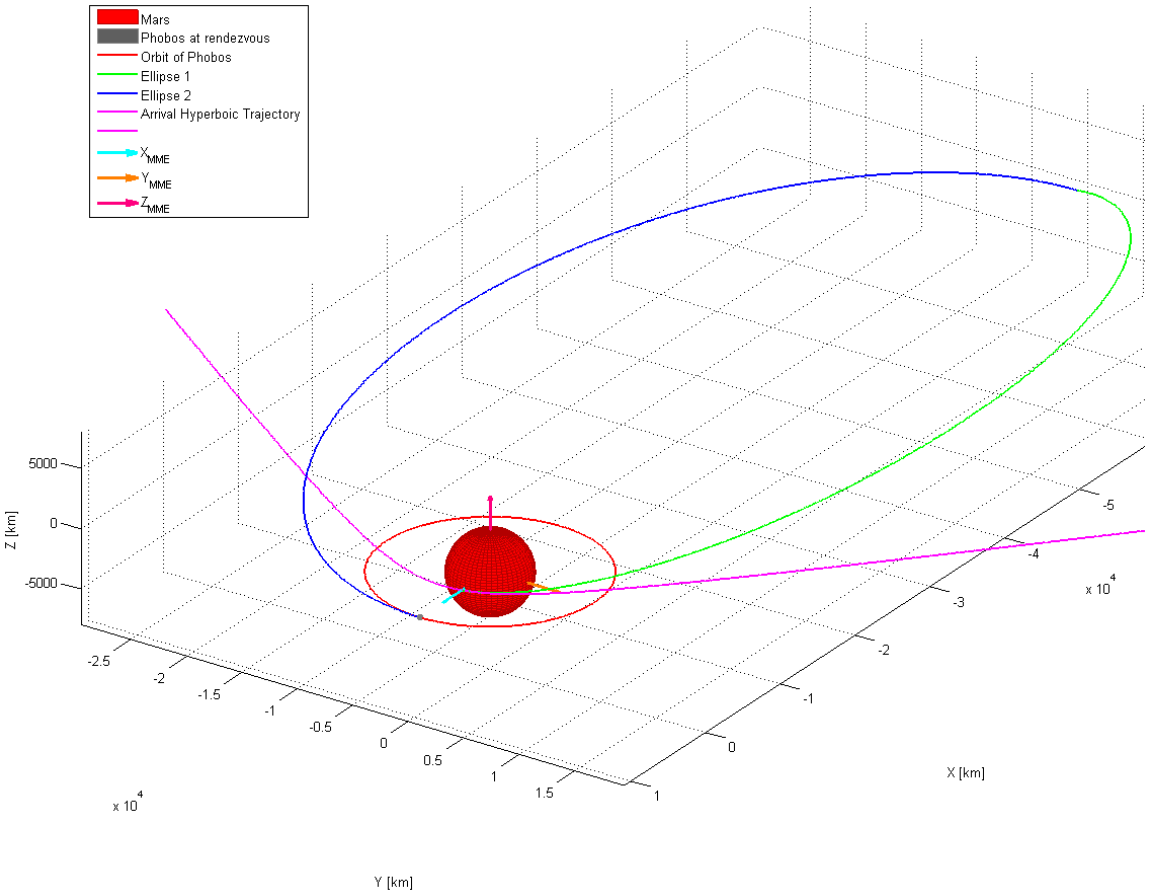

Figure 28 – Arrival scenario for the minimum ΔV case (2020-2022 timeframe) using a bi-elliptic transfer to rendezvous with Phobos.

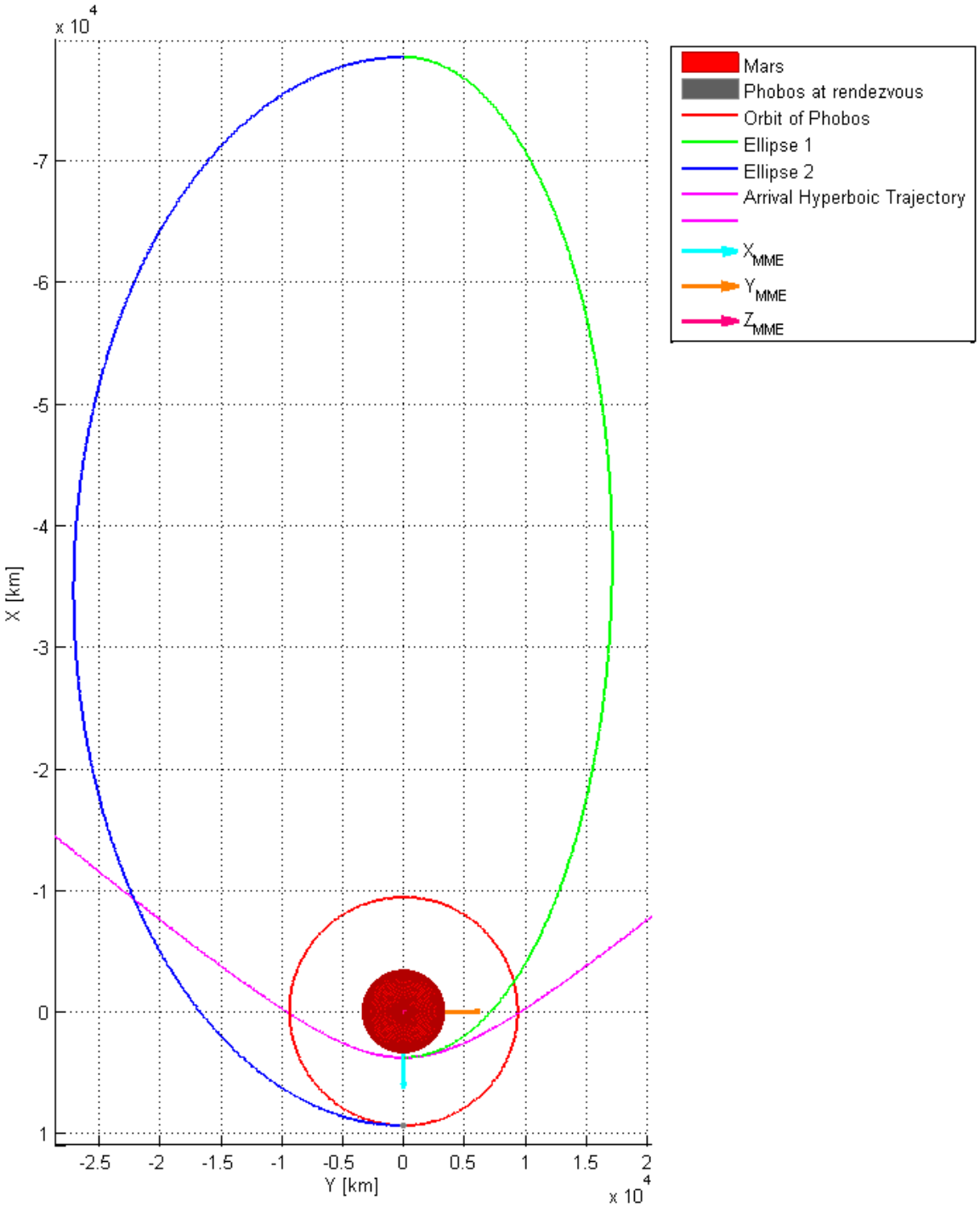

Figure 29 – Arrival scenario (top view) for the minimum ΔV case (2020-2022 timeframe) using a bi-elliptic transfer to rendezvous with Phobos.

Table 6 – Summary of comparison between the trajectory considered by Hopkins and the results of the 2020-2022 case 1 and case 2. The total ΔV was obtained assuming an Earth parking orbit altitude of 300 km. Source: Hopkins, p. 12.[5]

Earth-Phobos Trajectories – Comparison			
Parameter	**Hopkins' Results**	**Case 1**	**Case 2**
Departure Date	April 17, 2033	July 31, 2020	July 31, 2020
Arrival Date	November 4, 2033	February 27, 2021	February 27, 2021
Time of Flight	201 days	211 days	211 days
Loiter time in Mars orbit	49 days	17 days (max)	49 days
C3 at Launch	9.17 km^2/s^2	14.881 km^2/s^2	14.881 km^2/s^2
v_∞ at Arrival	3.317 km/s	2.5227 km/s	2.5227 km/s
Δv for capture and rendezvous with Phobos	2.017 km/s	1.840 km/s	1.575 km/s
Arrival i (MME)	9.60°	6.321°	6.321°
Arrival periapse altitude	400 km	6100 km	400 km
Apoapse altitude of bi-elliptic transfer	75000 km	N/A	75000 km
Δv_{tot} (including rendezvous maneuvers)	5.6291 km/s	5.6764 km/s	5.4114 km/s

Similar results to those reported in Table 6 can be obtained for minimum Δv trajectories of other timeframes. In fact, although the orbits of Earth and Mars around the Sun are not circular and coplanar, minimum Δv opportunities leading similar results to those of Table 6 occur periodically. Additionally, the same procedure can be applied to analyze arrival trajectories to rendezvous with Deimos. Note that the dates for case 1 and case 2 differ from those used by Hopkins since the 2020-2022 timeframe leads to the lowest total Δv cases. In fact, although the

minimum Δv cases roughly repeat every Earth-Mars synodic period (approximately 26 months), the actual values of minimum Δv vary depending on various factors such as the interplanetary inclination of the Earth-Mars transfer orbit. Appendix D reports the key results for various date combinations and for case 1 transfers.

Orbit Insertion about Phobos and Deimos

As mentioned in Chapter 1, the spheres of influence of the moons of Mars are below their surfaces. Therefore, it is not possible to analyze the arrival trajectory of a spacecraft at either Phobos or Deimos using the classical two-body problem equations. Instead, the strong perturbations of Mars must be included and the spacecraft orbit should be analyzed using the CR3BP relations for the Mars-Phobos or Mars-Deimos systems. In fact, upon arrival to one of the moons of Mars, orbits such as those shown in Figure 4 might be considered or a direct landing on the surface could be done. For more details, refer to Wallace, Parker, Strange, and Grebow.[21]

Chapter 7

Conclusions and Future Work

Conclusions

Although no missions to Phobos or Deimos have successfully been done, they are certainly within the capabilities that today's technology can offer. Porkchop plots are a great starting point for designing interplanetary missions. In fact, past missions such as Mariner 4[10], Mars Reconnaissance Orbiter (MRO) [11], Mars Science Laboratory (MSL)[12], and future missions such as Mars Atmosphere and Volatile EvolutioN (MAVEN)[14] made use of the minimum (or close to minimum) Δv_{tot} required to depart from Earth and arrive at Mars. A more difficult challenge is targeting a celestial body, such as Phobos, within the sphere of influence of a bigger body, such as Mars. In fact, Lambert's problem does not model the sphere of influence of the arrival body, and additional analysis is required to determine the arrival trajectory at Mars.

This thesis is not meant to be exhaustive in analyzing the problem of targeting Phobos and Deimos, but it rather offers an overview of some of the ways in which such problem can be approached. Alternatives were mentioned in Chapter 1.

Parameters such as Δv_{tot} and TOF may be weighted differently depending on whether a mission is robotic or human. In fact, in the case of a manned spacecraft, one of the primary concerns of a mission to Mars and/or Phobos is the time spent under the influence of interplanetary radiation. Therefore, a mission with higher Δv_{tot} but considerably much lower TOF may be considered. If targeting Phobos, for example, a propulsive maneuver at periapse like the one described in Chapter 5 may be preferable to make sure that the spacecraft is captured by Mars. On the other hand, a bi-elliptic transfer can be used to lower the Δv required, especially if time is not a key mission parameter, i.e. if the spacecraft is unmanned.

For a robotic mission with no specific time constraints, it is preferable to use a trajectory that minimizes the amount of propellant usage, i.e. minimize Δv_{tot}. In the 2020-2022 timeframe for an Earth-Phobos mission, it was found that the optimal departure and arrival dates are July 31, 2020 and February 27, 2021 respectively. The minimum Δv_{tot} does not correspond to the minimum inclination change, but it is a result of the combination of key parameters such as C3 at launch, v_∞ at arrival, the orientation of the MME reference frame for the particular arrival time considered, and the orientation of the Earth-Mars transfer orbit in the J200 ecliptic reference frame. From Table 6, it can be seen that case 1 and case 2 may be preferable than the scenario proposed by Hopkins for TOF and Δv_{tot} respectively.

The same analysis and algorithms described in this thesis can be used to generate results for any other timeframes and for Earth-Deimos missions.

Future Work

The work presented in this thesis is only a small portion of the analysis that would be done for a full mission to Phobos or Deimos. In fact, a greater level of accuracy should be used and other unmodeled forces such as solar radiation pressure should be included. Additionally, this thesis does not address the return to Earth trajectories which would be of interest particularly for a manned mission to Phobos or Deimos and for a sample return mission.

Another problem exists when considering Phobos or Deimos rendezvous. In fact, most orbits around the L_1 and L_2 points of Phobos and Deimos are unstable, making orbit insertion about the moons a major challenge.[21] In fact, although the instability of such orbits can be corrected via station-keeping maneuvers, such maneuvers must be performed frequently (in the order of hours) and very accurately. Perhaps a solution might make use of Distant Retrograde Orbits which tend to be stable in the Mars-Phobos and Mars-Deimos systems.[21]

Appendix A

Lambert Solution – Flowchart

The following flowchart outlines the key steps in solving the Lambert Problem.

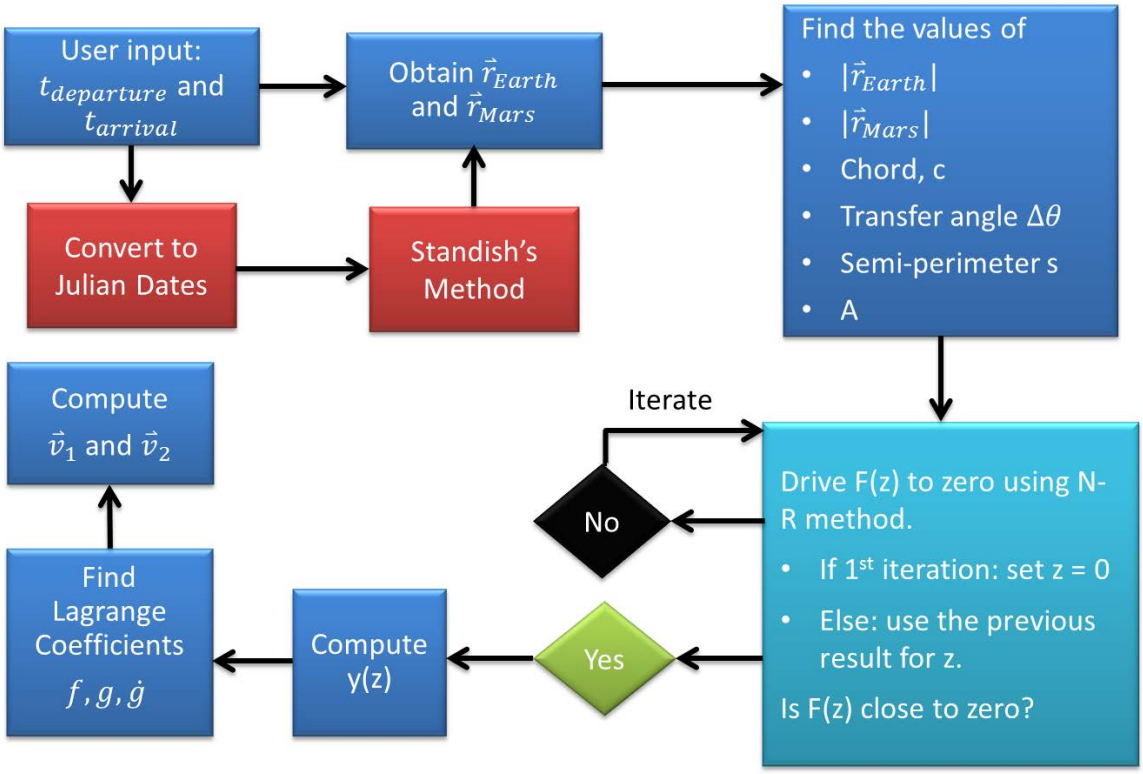

Figure A 1 – Flowchart showing the main steps when solving Lambert's problem.

Appendix B

Creating Porkchop Plots – Flowchart

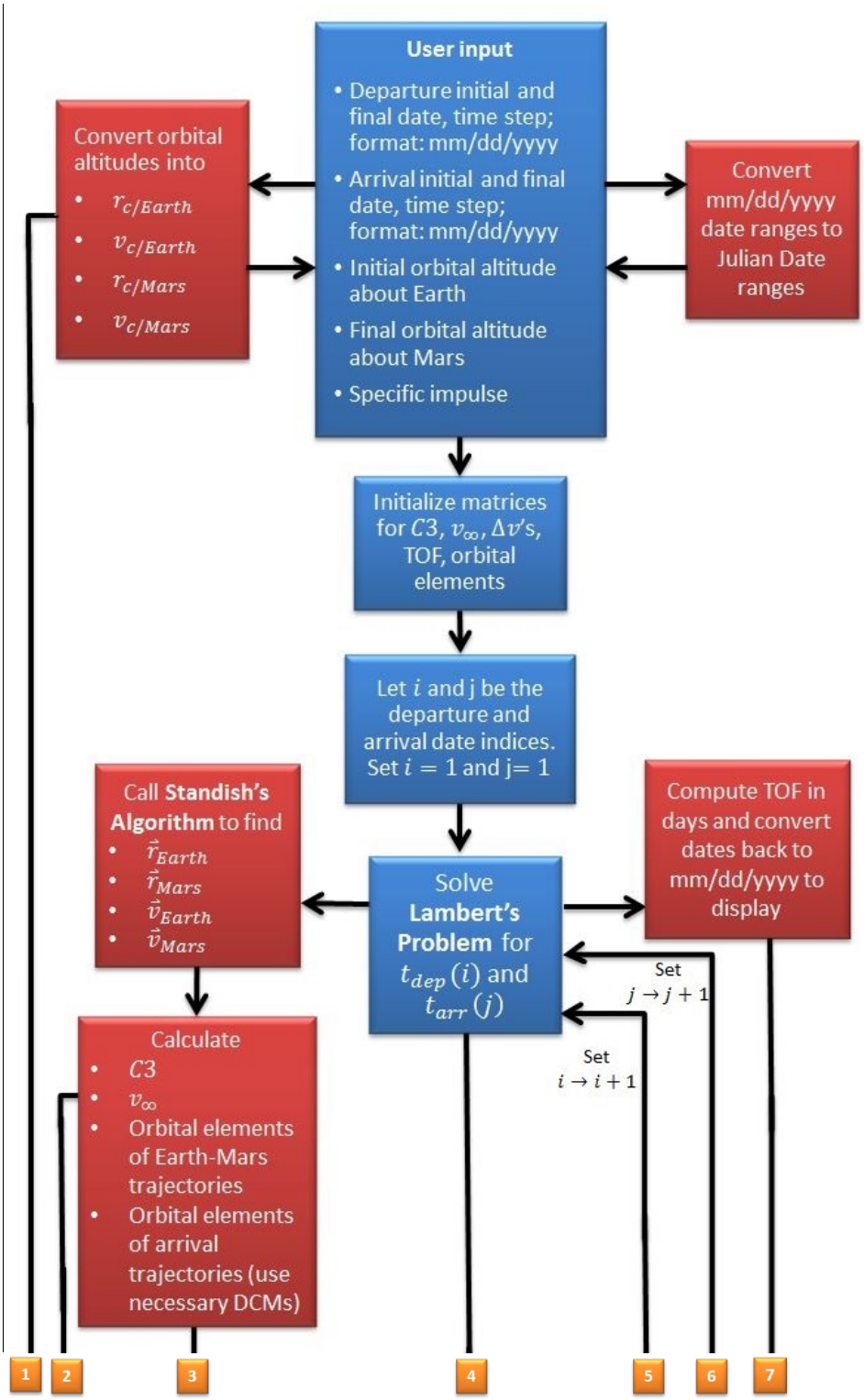

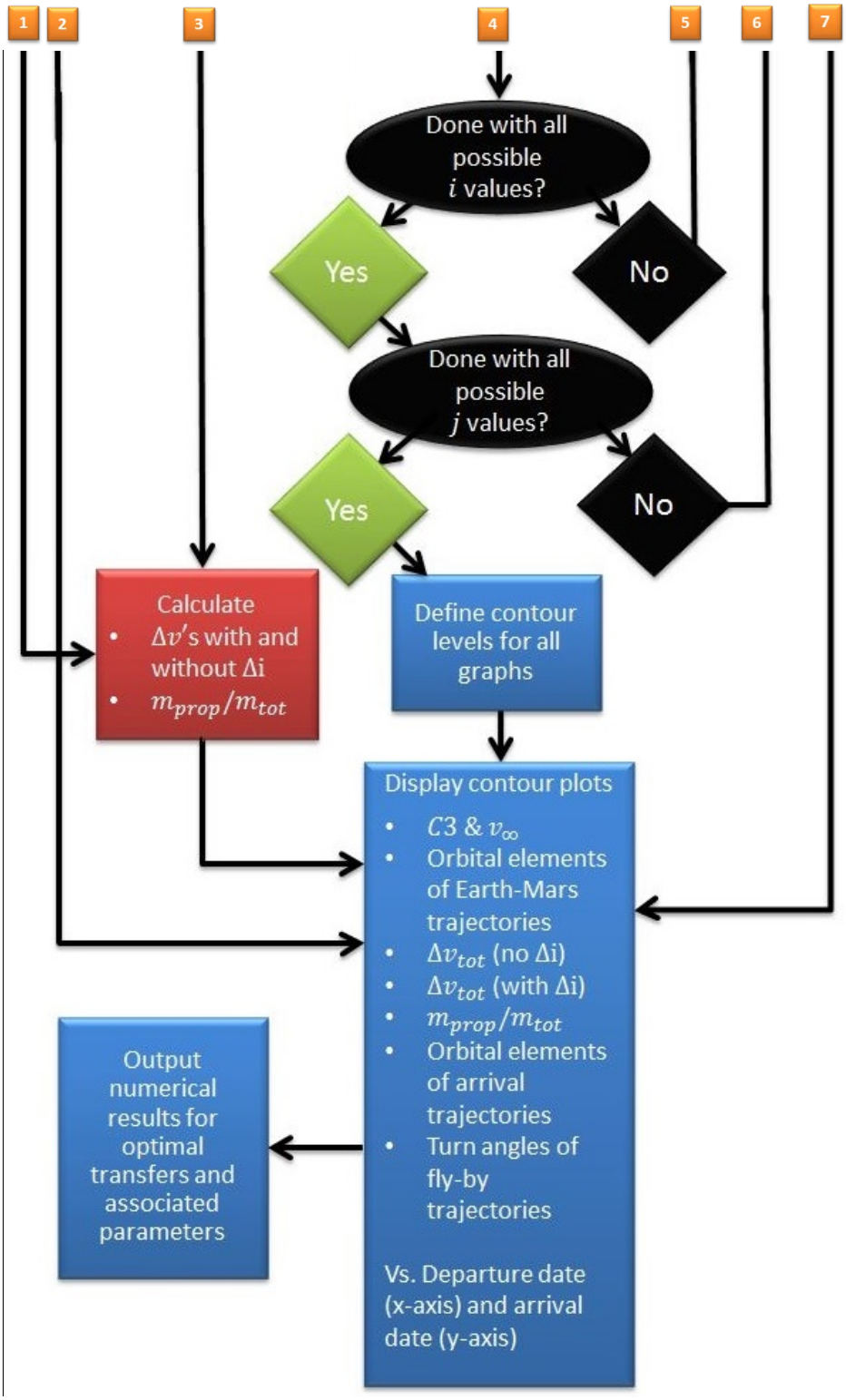

Figure B 1 – Flowchart showing the main steps when creating porkchop plots.

Appendix C

Computing Considerations

The algorithms shown in Figure A 1 and Figure B 1 were implemented in MATLAB. Because of the large amount of computations required to obtain the results shown throughout this thesis, the overall running time of the MATLAB main script and functions is on the order of hours if using a personal computer. Note that this does not represent a major obstacle since the time required to simulate thousands of trajectories is much less than any time of flight considered. On the other hand, if results of large ranges of departure and arrival times (2+ years each) are required, it is necessary to make sure that the code that has been developed is reliable in order to avoid wasting time debugging it. Various porkchop plots can be found on the NASA website and can be used to validate the Lambert's problem solver implemented in the computer code.

The major specifications of the personal computer used to generate the results of this thesis are presented in Table C 1. Table C 2 shows various examples of number of iterations vs. computing time. The number of iterations is defined as the product of the total departure days by the total arrival days that are being considered. For example, a 30x30 days departure/arrival combination would produce a total number of iterations of 900.

Table C 1 – Specifications of the personal computer used in this thesis.

Computer Specifications	
Manufacturer	Toshiba
Model	Satellite P70-A
Processor	Intel® Core™ i7-4700MQ CPU @ 2.40 GHz 2.40 GHz
Installed Memory (RAM)	16.0 Gb
System Type	64-bit Operating System, x64-based processor
Operating System	Windows 8

Table C 2 – Number of iterations vs. computing time

Number of Iterations vs. Computing Time			
Departure Date Range	**Arrival Date Range**	**Number of Iterations**	**Computing time (hours)**
6/1/2005 – 11/1/2005	1/1/2006 – 12/31/2006	66614	1.23
8/1/2011 – 2/28/2012	5/15/2012 – 3/15/2013	64144	1.19
7/15/2013 – 4/1/2014	5/1/2014 – 7/31/2016	86310	1.60
5/1/2020 – 11/15/2020	12/1/2020 – 1/31/2022	84348	1.57
3/1/2035 – 9/30/2035	10/15/2035 – 2/15/2037	104860	1.95

The average number of iterations/computing time was calculated to be approximately 15 iterations every second.

Appendix D

Arrival Trajectories – Details

Tables D1 – D25 give the maximum or minimum values of the key parameters of the sets of dates reported on Table C2. These results were obtained using the algorithms and computer code described throughout this thesis and can be used to analyze the arrival trajectories at Mars and compute the rendezvous trajectories with Phobos or Deimos. Note that generally most parameters are maximized (or minimized) for similar departure and arrival dates. The only exception is given by the inclination at Mars arrival with respect to the MME reference frame, making the Phobos or Deimos targeting particularly more challenging to predict than just an Earth-Mars transfer. In fact, as previously mentioned, the minimum inclination case generally does not correspond to the minimum Δv_{tot}.

Table D 1 – Earth-Mars trajectories: minimum launch C3 for the timeframe 2005-2006.

Earth-Mars Trajectories for the 2005-2006 timeframe – Minimum C3L	
Parameter	**Value**
Δv_{tot}	6.0338 km/s
C3 at Launch	15.447 km^2/s^2
v_∞ at Arrival	3.5109 km/s
Interplanetary a	1.3788 AU
Interplanetary e	0.269
Interplanetary i (J2000)	1.2061°
Interplanetary ω (J2000)	183.8°
Interplanetary Ω (J2000)	159.6°
Departure Date	September 2, 2005
Arrival Date	October 9, 2006
Time of Flight	402 days

Table D 2 – Earth-Mars trajectories: minimum v_∞ at Mars arrival for the timeframe 2005-2006.

Earth-Mars Trajectories for the 2005-2006 timeframe – Minimum v_∞ at arrival	
Parameter	**Value**
Δv_{tot}	6.3821 km/s
C3 at Launch	26.141 km^2/s^2
v_∞ at Arrival	2.3610 km/s
Interplanetary a	1.3196 AU
Interplanetary e	0.254
Interplanetary i (J2000)	2.8754°
Interplanetary ω (J2000)	332.46°
Interplanetary Ω (J2000)	−14.63°
Departure Date	September 8, 2005
Arrival Date	April 20, 2006
Time of Flight	224 days

Table D 3 – Earth-Mars trajectories: minimum Δv_{tot} (no inclination change upon arrival at Mars) for the timeframe 2005-2006.

Earth-Mars Trajectories for the 2005-2006 timeframe – Minimum Δv_{tot} (no inclination change upon arrival at Mars)	
Parameter	**Value**
Δv_{tot}	5.8138 km/s
C3 at Launch	18.399 km^2/s^2
v_∞ at Arrival	2.5278 km/s
Interplanetary a	1.3355 AU
Interplanetary e	0.246
Interplanetary i (J2000)	3.1517°
Interplanetary ω (J2000)	348.16°
Interplanetary Ω (J2000)	−30.10°
Departure Date	August 23, 2005
Arrival Date	March 30, 2006
Time of Flight	219 days

Table D 4 – Earth-Mars trajectories: minimum inclination with respect to the MME reference frame for the timeframe 2005-2006.

Earth-Mars Trajectories for the 2005-2006 timeframe – Minimum inclination to rendezvous with Phobos or Deimos	
Parameter	**Value**
Δv_{tot}	7.492 km/s
Arrival i (MME)	0.0003°
C3 at Launch	36.263 km^2/s^2
v_∞ at Arrival	3.8290 km/s
Interplanetary a	1.3586 AU
Interplanetary e	0.292
Interplanetary i (J2000)	1.3275°
Interplanetary ω (J2000)	220.07°
Interplanetary Ω (J2000)	112.58°
Departure Date	July 15, 2005
Arrival Date	September 2, 2006
Time of Flight	414 days

Table D 5 – Earth-Mars trajectories: minimum Δv_{tot} including an inclination change upon arrival for the timeframe 2005-2006 (case 1).

Earth-Mars Trajectories for the 2005-2006 timeframe – Minimum Δv_{tot} including inclination change upon arrival at Mars	
Parameter	**Value**
Δv_{tot}	6.2056 km/s
Arrival i (MME)	0.04827°
C3 at Launch	15.845 km^2/s^2
v_∞ at Arrival	3.2338 km/s
Interplanetary a	1.1.3689 AU
Interplanetary e	0.263
Interplanetary i (J2000)	1.8180°
Interplanetary ω (J2000)	188.36°
Interplanetary Ω (J2000)	148.95°
Departure Date	August 22, 2005
Arrival Date	September 10, 2006
Time of Flight	384 days

Table D 6 – Earth-Mars trajectories: minimum launch C3 for the timeframe 2011-2013.

Earth-Mars Trajectories for the 2011-2013 timeframe – Minimum C3L	
Parameter	**Value**
Δv_{tot}	5.5224 km/s
C3 at Launch	8.948 km^2/s^2
v_∞ at Arrival	2.7584 km/s
Interplanetary a	1.2541 AU
Interplanetary e	0.211
Interplanetary i (J2000)	1.5175°
Interplanetary ω (J2000)	7.97°
Interplanetary Ω (J2000)	45.10°
Departure Date	November 8, 2011
Arrival Date	August 31, 2012
Time of Flight	297 days

Table D 7 – Earth-Mars trajectories: minimum v_∞ at Mars arrival for the timeframe 2011-2013.

Earth-Mars Trajectories for the 2011-2013 timeframe – Minimum v_∞ at arrival	
Parameter	**Value**
Δv_{tot}	5.5564 km/s
C3 at Launch	9.004 km^2/s^2
v_∞ at Arrival	2.7042 km/s
Interplanetary a	1.2523 AU
Interplanetary e	0.210
Interplanetary i (J2000)	1.7593°
Interplanetary ω (J2000)	5.85°
Interplanetary Ω (J2000)	48.11°
Departure Date	November 11, 2011
Arrival Date	September 12, 2012
Time of Flight	306 days

Table D 8 – Earth-Mars trajectories: minimum Δv_{tot} (no inclination change upon arrival at Mars) for the timeframe 2011-2013.

Earth-Mars Trajectories for the 2011-2013 timeframe – Minimum Δv_{tot} (no inclination change upon arrival at Mars)	
Parameter	**Value**
Δv_{tot}	5.5214 km/s
C3 at Launch	8.978 km^2/s^2
v_∞ at Arrival	2.7044 km/s
Interplanetary a	1.2524 AU
Interplanetary e	0.210
Interplanetary i (J2000)	1.7013°
Interplanetary ω (J2000)	6.79°
Interplanetary Ω (J2000)	47.11°
Departure Date	November 10, 2011
Arrival Date	September 12, 2012
Time of Flight	307 days

Table D 9 – Earth-Mars trajectories: minimum inclination with respect to the MME reference frame for the timeframe 2011-2013.

Earth-Mars Trajectories for the 2011-2013 timeframe – Minimum inclination to rendezvous with Phobos or Deimos	
Parameter	**Value**
Δv_{tot}	35.061 km/s
Arrival i (MME)	0.0074°
C3 at Launch	499.2 km^2/s^2
v_∞ at Arrival	19.812 km/s
Interplanetary a	1.3055 AU
Interplanetary e	0.690
Interplanetary i (J2000)	3.6424°
Interplanetary ω (J2000)	117.02°
Interplanetary Ω (J2000)	26.10°
Departure Date	October 20, 2011
Arrival Date	March 12, 2013
Time of Flight	509 days

Table D 10 – Earth-Mars trajectories: minimum Δv_{tot} including an inclination change upon arrival for the timeframe 2011-2013 (case 1).

Earth-Mars Trajectories for the 2011-2013 timeframe – Minimum Δv_{tot} including inclination change upon arrival at Mars	
Parameter	**Value**
Δv_{tot}	6.7860 km/s
Arrival i (MME)	0.3541°
C3 at Launch	16.017 km^2/s^2
v_∞ at Arrival	3.9802 km/s
Interplanetary a	1.2571 AU
Interplanetary e	0.217
Interplanetary i (J2000)	4.500°
Interplanetary ω (J2000)	170.35°
Interplanetary Ω (J2000)	243.18°
Departure Date	November 26, 2011
Arrival Date	August 13, 2012
Time of Flight	261 days

Table D 11 – Earth-Mars trajectories: minimum launch C3 for the timeframe 2013-2016.

Earth-Mars Trajectories for the 2013-2016 timeframe – Minimum C3L	
Parameter	**Value**
Δv_{tot}	5.8838 km/s
C3 at Launch	8.778 km^2/s^2
v_∞ at Arrival	4.3947 km/s
Interplanetary a	1.2219 AU
Interplanetary e	0.196
Interplanetary i (J2000)	2.5987°
Interplanetary ω (J2000)	5.54°
Interplanetary Ω (J2000)	99.31°
Departure Date	December 31, 2013
Arrival Date	November 24, 2014
Time of Flight	328 days

Table D 12 – Earth-Mars trajectories: minimum v_∞ at Mars arrival for the timeframe 2013-2016.

Earth-Mars Trajectories for the 2013-2016 timeframe – Minimum v_∞ at arrival	
Parameter	**Value**
Δv_{tot}	6.7939 km/s
C3 at Launch	10.137 km^2/s^2
v_∞ at Arrival	3.1508 km/s
Interplanetary a	1.2097 AU
Interplanetary e	0.193
Interplanetary i (J2000)	2.4227°
Interplanetary ω (J2000)	21.17°
Interplanetary Ω (J2000)	65.76°
Departure Date	November 28, 2013
Arrival Date	September 20, 2014
Time of Flight	296 days

Table D 13 – Earth-Mars trajectories: minimum Δv_{tot} (no inclination change upon arrival at Mars) for the timeframe 2013-2016.

Earth-Mars Trajectories for the 2013-2016 timeframe – Minimum Δv_{tot} (no inclination change upon arrival at Mars)	
Parameter	**Value**
Δv_{tot}	5.8658 km/s
C3 at Launch	9.564 km^2/s^2
v_∞ at Arrival	3.1607 km/s
Interplanetary a	1.2104 AU
Interplanetary e	0.191
Interplanetary i (J2000)	2.7164°
Interplanetary ω (J2000)	16.28°
Interplanetary Ω (J2000)	71.84°
Departure Date	December 4, 2013
Arrival Date	September 24, 2014
Time of Flight	294 days

Table D 14 – Earth-Mars trajectories: minimum inclination with respect to the MME reference frame for the timeframe 2013-2016.

Earth-Mars Trajectories for the 2013-2016 timeframe – Minimum inclination to rendezvous with Phobos or Deimos	
Parameter	**Value**
Δv_{tot}	41.205 km/s
Arrival i (MME)	0.0018°
C3 at Launch	808.4 km^2/s^2
v_∞ at Arrival	20.374 km/s
Interplanetary a	1.8757 AU
Interplanetary e	0.764
Interplanetary i (J2000)	1.3789°
Interplanetary ω (J2000)	254.11°
Interplanetary Ω (J2000)	68.83°
Departure Date	December 19, 2013
Arrival Date	February 5, 2016
Time of Flight	778 days

Table D 15 – Earth-Mars trajectories: minimum Δv_{tot} including an inclination change upon arrival for the timeframe 2013-2016 (case 1).

Earth-Mars Trajectories for the 2013-2016 timeframe – Minimum Δv_{tot} including inclination change upon arrival at Mars	
Parameter	**Value**
Δv_{tot}	$6.7235\ km/s$
Arrival i (MME)	8.8746°
C3 at Launch	$16.506\ km^2/s^2$
v_∞ at Arrival	$3.8184\ km/s$
Interplanetary a	$1.2022\ AU$
Interplanetary e	0.205
Interplanetary i (J2000)	2.8398°
Interplanetary ω (J2000)	146.00°
Interplanetary Ω (J2000)	−58.35°
Departure Date	January 22, 2014
Arrival Date	September 3, 2014
Time of Flight	224 days

Table D 16 – Earth-Mars trajectories: minimum launch C3 for the timeframe 2020-2022.

Earth-Mars Trajectories for the 2020-2022 timeframe – Minimum C3L	
Parameter	**Value**
Δv_{tot}	5.8201 km/s
C3 at Launch	13.180 km^2/s^2
v_∞ at Arrival	2.8529 km/s
Interplanetary a	1.3285 AU
Interplanetary e	0.235
Interplanetary i (J2000)	1.5580°
Interplanetary ω (J2000)	0.47°
Interplanetary Ω (J2000)	−63.57°
Departure Date	July 19, 2020
Arrival Date	January 28, 2021
Time of Flight	193 days

Table D 17 – Earth-Mars trajectories: minimum v_∞ at Mars arrival for the timeframe 2020-2022.

Earth-Mars Trajectories for the 2020-2022 timeframe – Minimum v_∞ at arrival	
Parameter	**Value**
Δv_{tot}	5.8061 km/s
C3 at Launch	19.715 km^2/s^2
v_∞ at Arrival	2.4500 km/s
Interplanetary a	1.3089 AU
Interplanetary e	0.238
Interplanetary i (J2000)	2.1514°
Interplanetary ω (J2000)	337.40°
Interplanetary Ω (J2000)	−38.65°
Departure Date	August 14, 2020
Arrival Date	March 10, 2021
Time of Flight	208 days

Table D 18 – Earth-Mars trajectories: minimum Δv_{tot} (no inclination change upon arrival at Mars) for the timeframe 2020-2022.

Earth-Mars Trajectories for the 2020-2022 timeframe – Minimum Δv_{tot} (no inclination change upon arrival at Mars)	
Parameter	**Value**
Δv_{tot}	5.6544 km/s
C3 at Launch	14.382 km^2/s^2
v_∞ at Arrival	2.5479 km/s
Interplanetary a	1.3184 AU
Interplanetary e	0.231
Interplanetary i (J2000)	2.2504°
Interplanetary ω (J2000)	352.23°
Interplanetary Ω (J2000)	−53.99°
Departure Date	July 29, 2020
Arrival Date	February 22, 2021
Time of Flight	208 days

Table D 19 – Earth-Mars trajectories: minimum inclination with respect to the MME reference frame for the timeframe 2020-2022.

Earth-Mars Trajectories for the 2020-2022 timeframe – Minimum inclination to rendezvous with Phobos or Deimos	
Parameter	**Value**
Δv_{tot}	7.028 km/s
Arrival i (MME)	~0°
C3 at Launch	21.362 km^2/s^2
v_∞ at Arrival	4.0149 km/s
Interplanetary a	1.3901 AU
Interplanetary e	0.281
Interplanetary i (J2000)	2.0920°
Interplanetary ω (J2000)	166.38°
Interplanetary Ω (J2000)	170.40°
Departure Date	September 13, 2020
Arrival Date	October 15, 2021
Time of Flight	397 days

Table D 20 – Earth-Mars trajectories: minimum Δv_{tot} including an inclination change upon arrival for the timeframe 2020-2022 (case 1).

Earth-Mars Trajectories for the 2020-2022 timeframe – Minimum Δv_{tot} including inclination change upon arrival at Mars	
Parameter	**Value**
Δv_{tot}	$5.6764\ km/s$
Arrival i (MME)	6.321°
C3 at Launch	$14.881\ km^2/s^2$
v_∞ at Arrival	$2.5227\ km/s$
Interplanetary a	$1.3171\ AU$
Interplanetary e	0.231
Interplanetary i (J2000)	2.384°
Interplanetary ω (J2000)	350.61°
Interplanetary Ω (J2000)	−52.07°
Departure Date	July 31, 2020
Arrival Date	February 27, 2021
Time of Flight	211 days

Table D 21 – Earth-Mars trajectories: minimum launch C3 for the timeframe 2033-2035.

Earth-Mars Trajectories for 2033-2035 timeframe – Minimum C3L	
Parameter	**Value**
Δv_{tot}	5.5862 km/s
C3 at Launch	10.198 km^2/s^2
v_∞ at Arrival	2.6925 km/s
Interplanetary a	1.2844 AU
Interplanetary e	0.209
Interplanetary i (J2000)	0.5321°
Interplanetary ω (J2000)	0.28°
Interplanetary Ω (J2000)	−89.58°
Departure Date	June 23, 2035
Arrival Date	January 5, 2036
Time of Flight	196 days

Table D 22 – Earth-Mars trajectories: minimum v_∞ at Mars arrival for the timeframe 2033-2035.

Earth-Mars Trajectories for the 2033-2035 timeframe – Minimum v_∞ at arrival	
Parameter	**Value**
Δv_{tot}	5.5671 km/s
C3 at Launch	12.024 km^2/s^2
v_∞ at Arrival	2.6005 km/s
Interplanetary a	1.2830 AU
Interplanetary e	0.211
Interplanetary i (J2000)	1.0048°
Interplanetary ω (J2000)	346.75°
Interplanetary Ω (J2000)	−73.12°
Departure Date	July 10, 2035
Arrival Date	January 25, 2036
Time of Flight	199 days

Table D 23 – Earth-Mars trajectories: minimum Δv_{tot} (no inclination change upon arrival at Mars) for the timeframe 2033-2035.

Earth-Mars Trajectories for the 2033-2035 timeframe – Minimum Δv_{tot} (no inclination change upon arrival at Mars)	
Parameter	**Value**
Δv_{tot}	5.5332 km/s
C3 at Launch	10.461 km^2/s^2
v_∞ at Arrival	2.6238 km/s
Interplanetary a	1.2840 AU
Interplanetary e	0.209
Interplanetary i (J2000)	0.9288°
Interplanetary ω (J2000)	355.97°
Interplanetary Ω (J2000)	−83.64°
Departure Date	June 29, 2035
Arrival Date	January 17, 2036
Time of Flight	202 days

Table D 24 – Earth-Mars trajectories: minimum inclination with respect to the MME reference frame for the timeframe 2033-2035.

Earth-Mars Trajectories for the 2033-2035 timeframe – Minimum inclination to rendezvous with Phobos or Deimos	
Parameter	**Value**
Δv_{tot}	8.468 km/s
Arrival i (MME)	0.0003°
C3 at Launch	45.219 km^2/s^2
v_∞ at Arrival	4.5934 km/s
Interplanetary a	1.3308 AU
Interplanetary e	0.258
Interplanetary i (J2000)	8.4658°
Interplanetary ω (J2000)	332.05°
Interplanetary Ω (J2000)	−33.67°
Departure Date	August 20, 2035
Arrival Date	June 9, 2036
Time of Flight	294 days

Table D 25 – Earth-Mars trajectories: minimum Δv_{tot} including an inclination change upon arrival for the timeframe 2033-2035 (case 1).

Earth-Mars Trajectories for the 2033-2035 timeframe – Minimum Δv_{tot} including inclination change upon arrival at Mars	
Parameter	**Value**
Δv_{tot}	7.2170 km/s
Arrival i (MME)	0.1698°
C3 at Launch	24.227 km^2/s^2
v_∞ at Arrival	4.0846 km/s
Interplanetary a	1.2859 AU
Interplanetary e	0.211
Interplanetary i (J2000)	6.7965°
Interplanetary ω (J2000)	7.18°
Interplanetary Ω (J2000)	267.06°
Departure Date	June 19, 2035
Arrival Date	February 14, 2036
Time of Flight	240 days

BIBLIOGRAPHY

1. Burkhart, Daniel P. "MSL Update to Mars Coordinate Frame Definitions." *NASA JPL*. NASA JPL, 15 Aug. 2006. Web. 1 Feb. 2014. <http://soliton.ae.gatech.edu/people/rbraun/classes/astroI08/MSLCoordFrameMemo>.
2. Curtis, Howard D. *Orbital Mechanics for Engineering Students*, 2nd edition. Elsevier Aerospace Engineering Series, 2010.
3. Davis, Phil. "Solar System Exploration: Missions: In Flight." Solar System Exploration: Missions: In Flight. NASA, 2013. Web. 7 Aug. 2013. <http://solarsystem.nasa.gov/missions/profile.cfm?InFlight=1>.
4. Farquhar, Robert W., and Ahmed A. Kamel. "Quasi-periodic Orbits about the Translunar Libration Point." *Celestial Mechanics* 7.4 (1973): 458-73. Print.
5. Hopkins, Joshua, and William Pratt. "Comparison of Deimos and Phobos as Destinations for Human Exploration and Identification of Preferred Landing Sites." *AIAA SPACE 2011 Conference & Exposition* (2011), 29 Dec. 2011. Web. 15 Feb. 2014. <http://www.csc.caltech.edu/references/Hopkins-Phobos-Deimos-Paper.pdf>.
6. Hopkins, Joshua. "Deimos and Phobos as Destinations for Human Exploration." Caltech Space Challenge. Pasadena. Mar. 2013. Speech.
7. Jah, Moriba. "Derivation of the B-plane (Body Plane) and Its Associated Parameters." Jet Propulsion Lab, 2002. Web. 25 Jan. 2014. <http://cbboff.org/UCBoulderCourse/documents/b-plane.PDF>.
8. Kemble, Stephen. *Interplanetary Mission Analysis and Design*. Berlin: Springer in Association with Praxis, 2006. Print.
9. Lee, Pascal, and Gary L. Martin. "Human Missions to Phobos and Deimos: What Science?" Mars Institute and SETI Institute, 2011. Web. 15 Feb. 2014. <http://multimedia.seti.org/PhD2011/abstracts/PhD2-11-001.pdf>.

10. "Mariner 3 & 4." *Mars Exploration Program*. NASA JPL, 2009. Web. 10 Oct. 2013. <http://mars.jpl.nasa.gov/programmissions/missions/past/mariner34/>.
11. "Mars Reconnaissance Orbiter." *Mars Reconnaissance Orbiter*. NASA JPL, 2009. Web. 10 Oct. 2013. <http://mars.jpl.nasa.gov/mro/>.
12. "Mars Science Laboratory." *Mars Science Laboratory*. NASA JPL, 2009. Web. 10 Oct. 2013. <http://mars.jpl.nasa.gov/msl/>.
13. "MATLAB." *MATLAB - The Language of Technical Computing*. MathWorks, 2013. Web. 10 Sept. 2013. <http://www.mathworks.com/products/matlab/>.
14. "MAVEN." *Mars Exploration Program*. NASA JPL, 2013. Web. 10 Oct. 2013. <http://mars.jpl.nasa.gov/programmissions/missions/future/maven/>.
15. "NASA's Mars Exploration Program." *Mars Exploration: Features*. NASA JPL, 2013. Web. 10 Nov. 2013. <http://mars.jpl.nasa.gov/spotlight/porkchopAll.html>.
16. "Phobos, One of the Two Moons of Mars, In-situ with Samples Return." *Mission Phobos-Grunt*. CNES, 12 Sept. 2011. Web. 15 Feb. 2014. <http://smsc.cnes.fr/PHOBOS/GP_mission.htm>.
17. Prussing, John E., and Bruce A. Conway. *Orbital Mechanics*. New York: Oxford UP, 1993. Print.
18. Robbins, W.H. and Finger, H.B., "An Historical Perspective of the NERVA Nuclear Rocket Engine Technology Program", NASA Contractor Report 187154/AIAA-91-3451, NASA Lewis Research Center, NASA, July 1991.
19. Standish, Erland M., “Keplerian Elements for Approximate Position of the Major Planets.” NASA JPL, 2006. Print.
20. Vallado, David A. *Fundamentals of Astrodynamics and Applications*. 3rd ed. Dordrecht: Kluwer Academic, 2007. Print.

21. Wallace, Mark S., Jeffrey S. Parker, Nathan J. Strange, and Daniel Grebow. *Orbital Operations for Phobos and Deimos Exploration*. Tech. Jet Propulsion Lab, 13 Aug. 2012. Web. 01 Mar. 2014. <http://trs-new.jpl.nasa.gov/dspace/bitstream/2014/43035/1/12-3712_A1b.pdf>.
22. Wertz, James R., David F. Everett, and Jeffery Puschell. *Space Mission Engineering: The New SMAD.* Page 207 Microcosm Press and Springer, 2011.
23. Williams, David R. "Mars Fact Sheet." *Mars Fact Sheet*. NASA, 1 Jul. 2013. Web. 7 Feb. 2014. <http://nssdc.gsfc.nasa.gov/planetary/factsheet/marsfact.html>.
24. Yeomans, Donald K. "Keplerian Elements for Approximate Positions of the Major Planets."Keplerian Elements for Approximate Positions of the Major Planets. NASA JPL, 11 Mar. 2011. Web. 09 Aug. 2013. <http://ssd.jpl.nasa.gov/?planet_pos>.